bioRxiv preprint doi: https://doi.org/10.1101/2020.07.23.217216; this version posted July 24, 2020. The copyright holder for this preprint (which was not certified by peer review) is the author/funder, who has granted bioRxiv a license to display the preprint in perpetuity. It is made available under a CC-BY 4.0 International License.

Non-synaptic interactions between olfactory receptor neurons, a possible key-feature in insect odor inspection

Mario Pannunzi[1*] **and Thomas Nowotny**[1]

***For correspondence:**
mario.pannunzi@gmail.com (MP);
t.nowotny@sussex.ac.uk (TN)

[1]School of Engineering and Informatics, University of Sussex, Brighton, UK

Abstract When flies explore their environment, they encounter odors in complex, highly intermittent plumes. To navigate a plume and, for example, find food, flies must solve several tasks, including reliably identifying mixtures of odorants and discriminating odorant mixtures emanating from a single source from odorants emitted from separate sources and mixing in the air. Lateral inhibition in the antennal lobe is commonly understood to help solving these two tasks. With a computational model of the *Drosophila* olfactory system, we analyze the utility of an alternative mechanism for solving them: Non-synaptic ("ephaptic") interactions (NSIs) between olfactory receptor neurons that are stereotypically co-housed in the same sensilla. For both tasks, NSIs improve the insect olfactory system and outperform the standard lateral inhibition mechanism in the antennal lobe. These results shed light, from an evolutionary perspective, on the role of NSIs, which are normally avoided between neurons, for instance by myelination.

Introduction

Flies, as most other insects, rely primarily on olfaction to find food, mates, and oviposition sites. During these search behaviours, they encounter complex plumes with highly intermittent odor signals: Odor whiffs are infrequent and odor concentration varies largely between whiffs (***Yee et al., 1993***, ***1995***; ***Mylne and Mason, 1991***). To navigate a plume and successfully reach their objectives, flies must decipher these complex odor signals which includes several tasks: Identifying odors, whether mono-molecular or a mixture; Identifying odor intensity; Discriminating odorant mixtures emanating from a single source from those emanating from separate sources; identifying source locations, etc. Early sensory processing is understood to play an important role for completing these tasks. For instance, lateral inhibition in the antennal lobe is commonly understood to be useful for decorrelating odor signals from co-activated receptor types. Here we investigate the hypothesis that the early interactions between ORNs in the sensilla are similarly, if not more, useful for decoding information in odor plumes.

In both, vertebrates and invertebrates, odors are sensed by an array of numerous receptor neurons, each typically expressing receptors of exactly one of a large family of olfactory receptor (OR) types. In insects, olfactory receptor neurons (ORNs) are housed in evaginated sensilla localized on the antennae and maxillary palps (***Wilson, 2013***), each sensillum containing one to four ORNs of different types (***Todd and Baker, 1999***; ***Wilson, 2013***). The co-location of ORN types within the sensilla is stereotypical, i.e. ORNs of a given type “a” are always co-housed with ORNs of a specific type “b”. Furthermore, ORNs within the same sensillum can interact (***Shimizu and Stopfer, 2012***;

bioRxiv preprint doi: https://doi.org/10.1101/2020.07.23.217216; this version posted July 24, 2020. The copyright holder for this preprint (which was not certified by peer review) is the author/funder, who has granted bioRxiv a license to display the preprint in perpetuity. It is made available under a CC-BY 4.0 International License.

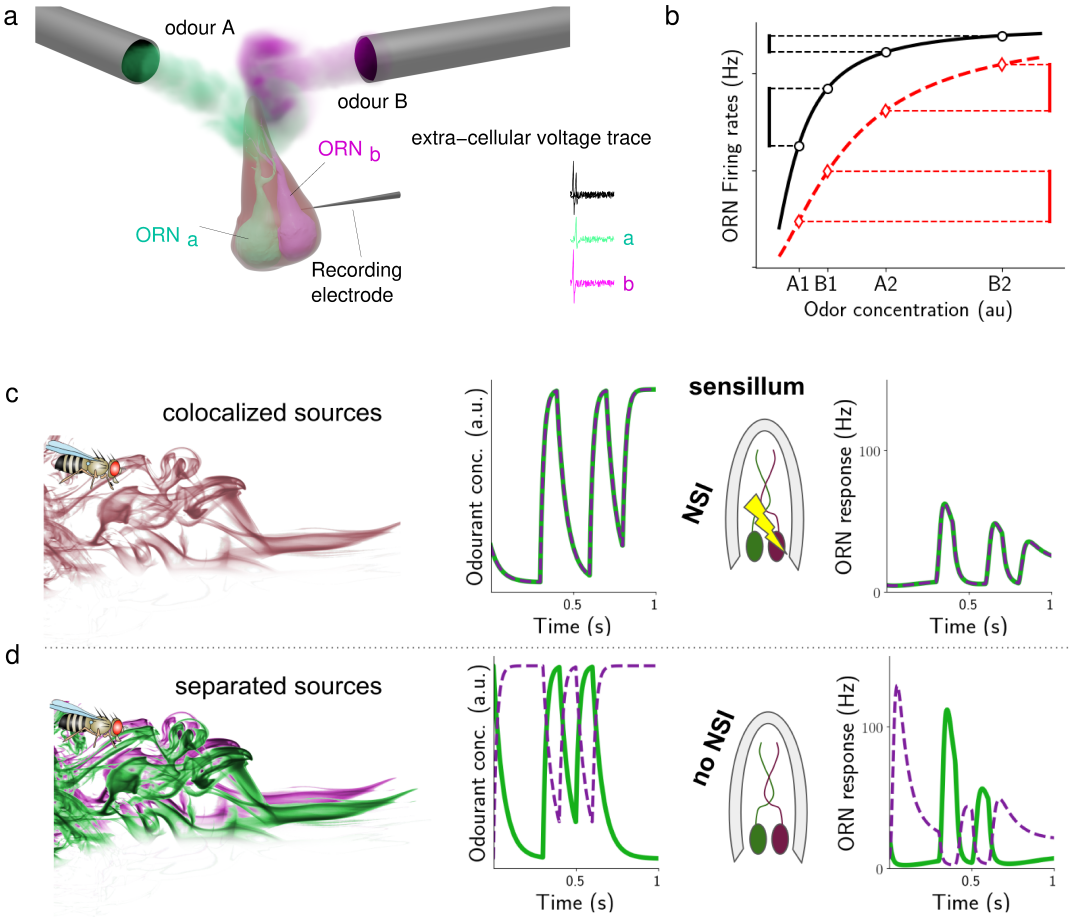

Figure 1. a) NSI interaction Theoretical and experimental studies have proposed that the non-synaptic interaction (NSI) between ORNs is mediated by a direct electrical field interaction between such closely apposed neurons. b) Hypothesis n.1: An inhibitory mechanism can increase the dynamic range of the ORNs and help to correctly encode the ratio between odorants even at high concentration. At low concentration, the ratio of two odorants (A1 and B1) can be encoded by ORNs, with and w/o NSI; when concentration is high (A2 and B2), the ORNs response without NSI is flatted on similar values and the ratio cannot be encoded. Hypothesis n.2: If a single source emits an odorant mixture (c), odorants will arrive in close synchronization, NSIs will take effect and the response in both ORNs is affected. If separate sources emit the odorants (d), they will arrive in a less correlated way (***Erskine, 2018***), and NSIs have almost no effect, resulting in larger ORN responses. ORN response data shown is based on a preliminary model.

Su et al., 2012; ***Todd and Baker, 1999***; ***Xu et al., 2019***; ***Zhang et al., 2019***) without making synaptic connections (see ***Figure 1***a). While the interactions are sometimes called "ephaptic", referring to their possible electronic nature, we here prefer to call them non-synaptic interactions (NSIs), for the sake of generality. Whether stereotypical co-location of - and NSIs between - ORNs have functions in olfactory processing and what these functions might be remains unknown, even though several non-exclusive hypotheses have been formulated (see e.g. ***Todd and Baker*** (***1999***) and references therein).

Here, we investigate two hypotheses: First, NSIs could help the olfactory system to identify ratios of odorant concentrations in mixtures more faithfully by enhancing the dynamic range of ORN responses (see ***Figure 1***, panel b). Second, NSIs could help improve the spatiotemporal resolution of odor recognition in complex plumes (see ***Figure 1***, panels c-d). In both hypotheses, the NSI mechanism has to compete with lateral inhibition in the antennal lobe, which is commonly recognized to fulfill these roles, even though, of course, the two mechanisms are not mutually exclusive. Indirect support for the first hypothesis is found in the context of moths' pheromone communication.

bioRxiv preprint doi: https://doi.org/10.1101/2020.07.23.217216; this version posted July 24, 2020. The copyright holder for this preprint (which was not certified by peer review) is the author/funder, who has granted bioRxiv a license to display the preprint in perpetuity. It is made available under a CC-BY 4.0 International license.

In some moth species, pheromone mixture ratio discrimination is critical for survival and therefore even slight changes in pheromone component ratios of 1-3% can cause significant changes in behavior. In these species, the ORNs responding to pheromone components are more likely to be co-housed. Meanwhile, when mixture ratios are not as critical for behavior, i.e., significant changes in behavior only occur if pheromone component ratios change 10% or more, ORNs are less likely to be paired in the same sensilla (see ***Todd and Baker*** (***1999***) and reference therein). The idea of extending dynamic range is a cornerstone for signal processing and metrology and we can find evidence for extended dynamics range in several senses, including olfaction (see e.g. ***Vermeulen and Rospars*** (***2004***); ***Reddy et al.*** (***2018***); ***Singh et al.*** (***2019***)): When a quantity of interest is encoded by neuronal activity through a sigmoid function (see ***Olsen et al.*** (***2010***) for an example for projectory neuron (PN) activity), the encoding has a limited dynamic range (see ***Figure 1***, panel b) that is determined by the shape of the sigmoid and the maximum firing rate of the neurons. A common neuronal strategy to increase the dynamic range in this situation is mutual inhibition between neurons, like that one taking place between PNs inside the antennal lobe (AL) (see e.g. ***Wilson*** (***2013***). We propose that NSIs in the sensilla implement such a mechanism and analyse how it improves the encoding of the concentration ratio of odor mixtures in PNs.

The improvement of spatiotemporal resolution of the second hypothesis can be achieved by decorrelating odor response profiles to improve odor recognition (see ***Figure 1***, panels c-d), much like lateral inhibition in the antennal lobe (AL), or centre-surround inhibition in the retina. Odorants dissipate in the environment in complex, turbulent plumes of thin filaments of a wide range of concentrations, intermixed with clean air. Odorants emanating from the same source presumably travel together in the same filaments while odorants from separate sources are in separate strands (see e.g., ***Erskine*** (***2018***) for empirical evidence for this intuitive idea). Insects are able to resolve odorants in a blend and recognize whether odorants are present in a plume and whether or not they belong to the same filaments (***Fadamiro and Baker, 1997***; ***Baker et al., 1998***; ***Krofczik et al., 2009***; ***Szyszka et al., 2012***). In the pheromone sub-system of moths, it is known that animals are able to detect, based on fine plume structure, whether multiple odorants have been emitted from the same source or not (***Fadamiro and Baker, 1997***; ***Baker et al., 1998***; ***Andersson et al., 2010***). In the pheromone subsystem of *Drosophila*, ORNs responding to chemicals emitted by virgin females and ORNs responding to chemicals emitted by mated females are co-housed in the same sensilla: The 'virgin females ORNs' promote male approach behavior, but the 'mated females ORNs' inhibit 'virgin females ORNs' (***van Naters and Carlson, 2007***). This inhibition could be implemented through NSIs (***Todd and Baker, 1999***; ***van Naters and Carlson, 2007***; ***Couto et al., 2005***; ***Binyameen et al., 2014***).

The experimental evidence for both hypotheses and for the general relevance of NSIs for olfactory processing remains mixed and research is still at an early stage. Encouraged by the available evidence, and without trying to rule out other hypotheses (for further analysis see Discussion), our goal is to investigate, with a computational model, the viability of the hypothesized function of NSIs between ORNs. Our computational approach helps experimental studies to refine hypotheses about NSI and eventually answer the pertinent question why such a mechanism that appears to duplicate what is already known to be implemented by local neurons in the AL (***Todd and Baker, 1999***) could nevertheless provide an evolutionary advantage.

A number of computational models have been developed to capture different aspects of the olfactory system of insects. However, until recently, most modeling efforts were based on the assumption of continuous constant stimuli, which are partially realistic only for non-turbulent fluid dynamics regimes (see (***Pannunzi and Nowotny, 2019***), and reference therein). Most commonly insects encounter turbulent regimes, in which odorant concentration fluctuates rapidly (see ***Figure 6–Figure Supplement 2***).

To cope with these more realistic stimuli, ***Kim et al.*** (***2011***); ***Lazar and Yeh*** (***2020***); ***Gorur-Shandilya et al.*** (***2017***); ***Jacob et al.*** (***2017***) have formulated new models of *Drosophila* ORNs, that are constrained by experimental data obtained with more rich, dynamic odor inputs, including a model

bioRxiv preprint doi: https://doi.org/10.1101/2020.07.23.217216; this version posted July 24, 2020. The copyright holder for this preprint (which was not certified by peer review) is the author/funder, who has granted bioRxiv a license to display the preprint in perpetuity. It is made available under a CC-BY 4.0 International license.

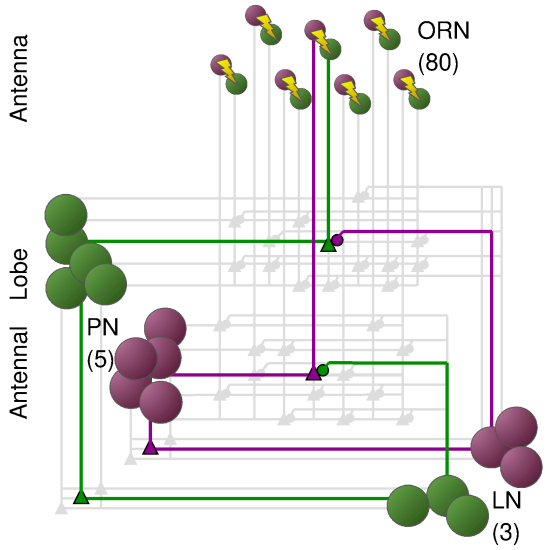

Figure 2. The model consists of a subset of the early olfactory system of insects from ORNs to the AL using only two groups of ORNs (ORN_a and ORN_b) and their respective PNs and LNs. Each ORN type, a and b, is tuned to a specific set of odorants (e.g. individual pheromone component) and converges onto its corresponding PNs. PNs impinge into their respective LNs, but receive inhibitory input from LNs of the other type.

simulating ORNs and PNs that are subject to input from simulated plumes (***Jacob et al., 2017***) with statistical properties akin to those of naturalistic plumes (see more details in Model and methods and Correlation detection in long realistic plumes).

Here, we present a network model with two groups of ORNs, each tuned to a specific set of odorants, connected to their corresponding glomeruli, formed by lateral neurons (LNs) and PNs, following the path started by ***Av-Ron and Rospars*** (***1995***); ***Av-Ron and Vibert*** (***1996***), and subsequently by ***Getz and Lutz*** (***1999***); ***Serrano et al.*** (***2013***); ***Zavada et al.*** (***2011***). We model the ORNs in a similar approach as ***Kim et al.*** (***2011***); ***Lazar and Yeh*** (***2020***) with minor differences in the filter properties and the adaptation (see Model and methods). We have tested the behavior of this network in response to simple reductionist stimuli (as commonly used in the literature, see above), and simulated naturalistic mixtures plumes (as described by the experiments in ***Mylne and Mason*** (***1991***); ***Yee et al.*** (***1995***)). We then used this simple but well-supported model to investigate the role of NSIs for odor mixture recognition.

Results

To investigate the role of NSIs in olfactory sensilla, we have built a computational model of the first two processing stages of the *Drosophila* olfactory system. In the first stage, ORN responses are described by an odor transduction process and a spike generator (see Model and methods), in line with previous experimental and theoretical studies (***Kim et al., 2011***, ***2015***; ***Martelli et al., 2013***; ***Lazar and Yeh, 2020***). We simulated pairs of ORNs expressing different OR types, as they are co-housed in sensilla. NSIs between co-housed pairs effectively lead to their mutual inhibition (see ***Figure 1***a). The second stage of olfactory processing occurs in the AL, in which PNs receive input from ORNs and form local circuits through LNs. ORNs of the same type all make excitatory synapses onto the same associated PNs. PNs excite LNs which then inhibit PNs of other glomeruli but not the PNs in the same glomerulus (see ***Figure 2*** and Model and methods for further details).

For maximum clarity, we here focus on only one type of sensillum and hence two types of ORNs that we denote as ORN_a and ORN_b. We further assume that odorants labeled A and B selectively activate ORN_a and ORN_b, respectively (see ***Figure 2*** and ***Figure 1***a). This assumption is not only sensible for a reductionist analysis of the role of NSIs, but it is also based on experimental observations. For instance, pheromone receptors in moths and in *Drosophila* are highly selective, paired

bioRxiv preprint doi: https://doi.org/10.1101/2020.07.23.217216; this version posted July 24, 2020. The copyright holder for this preprint (which was not certified by peer review) is the author/funder, who has granted bioRxiv a license to display the preprint in perpetuity. It is made available under a CC-BY 4.0 International license.

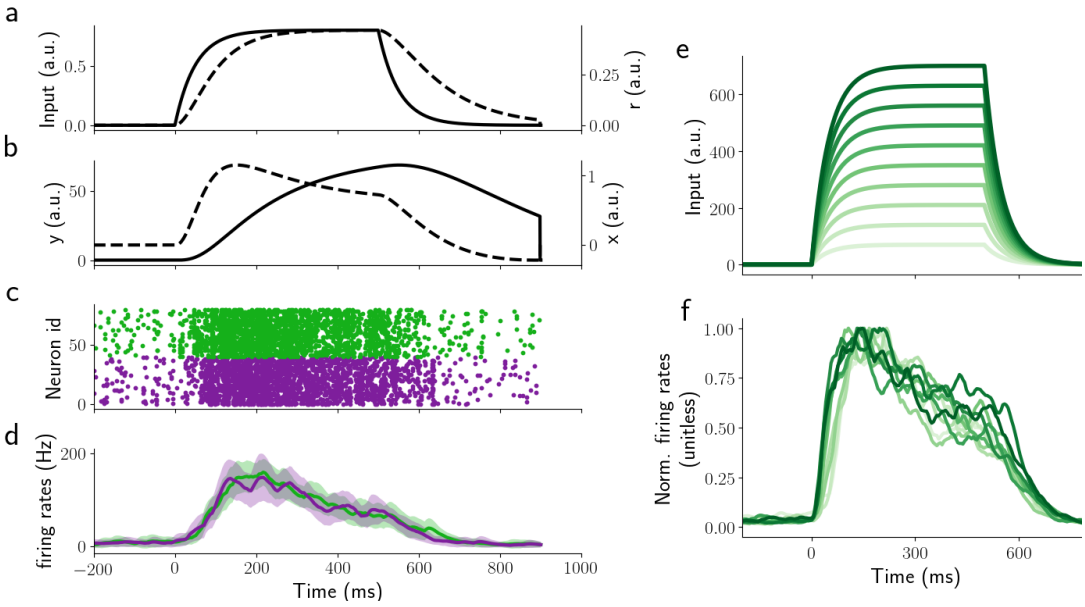

Figure 3. ORN responses to a 500ms single step stimulus. a) Stimulus waveform (continuous line) and receptor activation r (dashed). b) Activity of the internal ORN variables x (continuous) and y (dashed) (see Model and methods). c) Example spike raster of the spiking response of all 80 ORNs. d) Spike density function of the ORN population activity. The Shaded area represents the standard deviation across the ORNs of the same type. Color code for panels c-d: green for ORN_a and purple for ORN_b. e) Stimulus waveforms for different odorant concentrations. f) ORN activity normalized to the peak activity. odor concentration is indicated with different shades of green. After normalization, the responses are almost identical to those reported by ***Martelli et al.*** (***2013***).

Figure 3–Figure supplement 1. Model ORN response to a single step, a ramp, and a parabola as in (***Lazar and Yeh, 2020***).

Figure 3–Figure supplement 2. Output of the model of Lazar and Yeh (***Lazar and Yeh, 2020***) for comparison.

in sensilla, and exhibit NSIs (***Leal, 2013***; ***Todd and Baker, 1999***). In the general olfactory system of *Drosophila*, neurons ab3A and ab3B in sensillum ab3 are selectively sensitive to 2-heptanone and Methyl hexanoate, and when stimulated simultaneously they inhibit each other through NSIs (***Su et al., 2012***).

Constraining the ORN model to biophysical evidence

In this investigation we are particularly interested in the complex time course of odorant responses and have therefore focused on replicating realistic temporal dynamics of the response of ORNs at multiple time scales. ORN responses were constrained with experimental data obtained with delta inputs, i.e. inputs of very short duration and very high concentration, and random Gaussian pulses, i.e. series of input pulses which durations and inter-stimulus-intervals were drawn from a Gaussian distribution. We found that our model reproduces the data to a similar quality (relative error of around 6%) as previous linear-nonlinear models (***Kim et al., 2011***, ***2015***; ***Martelli et al., 2013***; ***Nagel and Wilson, 2011***; ***Lazar and Yeh, 2020***), even though it has fewer free parameters (see ***Figure 3***).

To further constrain the model, we compared its results to electrophysiological recordings from ORNs (***Kim et al., 2011***, ***2015***) responding to 2 s long odor stimuli with shapes resembling steps, ramps, and parabolas (see ***Figure 3–Figure Supplement 1*** and Model and methods). The model reproduces all key properties of the experimentally observed ORN responses. For the step stimuli, ORN activity peaks around 50ms after stimulus onset and the peak amplitude correlates with the odor concentration (***Figure 3–Figure Supplement 1***b). After the peak, responses gradually decrease to a plateau. Furthermore, if normalised by the peak value, responses have the same shape independently of the intensity of the stimulus (***Martelli et al., 2013***), see ***Figure 3***e,f. For the ramp

bioRxiv preprint doi: https://doi.org/10.1101/2020.07.23.217216; this version posted July 24, 2020. The copyright holder for this preprint (which was not certified by peer review) is the author/funder, who has granted bioRxiv a license to display the preprint in perpetuity. It is made available under a CC-BY 4.0 International License.

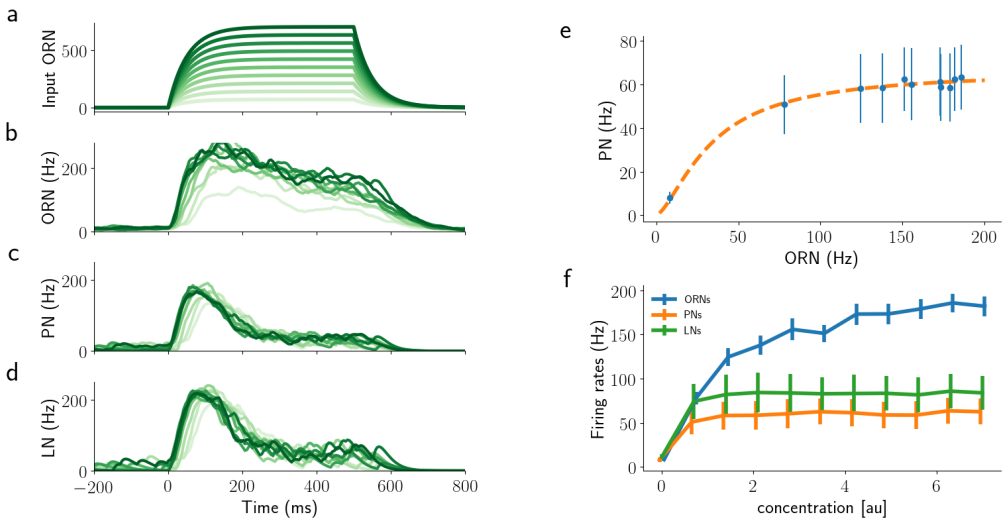

Figure 4. Network response to 500 ms step stimuli of a single odorant for the network as shown in ***Figure 2***. a) Step stimuli, shade of green indicates concentration. b)-d) corresponding activity of ORNs, PNs, and LNs. Shades of green match the input concentrations. e) Average response of PNs over 500 ms against the average activity of the corresponding ORNs. The orange dashed line is the fit of the simulated data using equation eq.1 as reported in (***Olsen et al., 2010***). f) Average values for PNs, ORNs, and LNs for different values of concentration. Error bars show the SE over PNs.

Figure 4–Figure supplement 1. Similar results for shorter stimulation time (50 ms).

Figure 4–Figure supplement 2. Similar results for shorter stimulation time (100 ms).

stimuli, ORN responses plateau after an initial period of around 200 ms, encoding the steepness of the ramp (***Figure 3–Figure Supplement 1***d). More generally, ORN responses seem to encode the rate of change of the stimulus concentration (***Kim et al., 2011***, ***2015***; ***Nagel and Wilson, 2011***). Accordingly, ORN activity in response to the parabolic stimuli is like a ramp (***Figure 3–Figure Supplement 1***f).

Model behavior for an isolated stimulus

Without further constraining the model we then tested PN responses with a single constant step stimulus. ***Olsen et al.*** (***2010***) reported that the response of PNs to such a stimulus is best described by a sigmoid,

$$\nu_{\mathrm{PN}} = \nu_{\max} \frac{\nu_{\mathrm{ORN}}^{1.5}}{\sigma^{1.5} + \nu_{\mathrm{ORN}}^{1.5}} \tag{1}$$

where $\nu_{\max}$ is the maximum firing rate of ORNs, σ is a fitted constant representing the level of ORN input that drives half-maximum response, and ν_{ORN} and ν_{PN}, are the average firing rates of the ORNs and the PN over the stimulation period (500 ms), respectively. Our model reproduces this behavior as a direct consequence of the model structure without any further parameter tuning (***Figure 4***). LNs follow the same behavior (see ***Figure 4***f). Note that this result, i.e. the sigmoidal behavior, generalizes to both, shorter stimulation times (50 and 100 ms, see ***Figure 4–Figure Supplement 1*** and ***Figure 4–Figure Supplement 2***) and to the peak activity instead of the time averaged activity (data not shown).

With a model in place that demonstrates the correct response dynamics for a variety of stimuli, we then analysed its predictions on whether NSIs can be beneficial for odor mixture processing. In particular, we tested the following two hypotheses: 1. Do NSIs improve the encoding of concentration ratio in an odorant mixture (see section Odorant ratio in synchronous mixture stimuli) and 2. Do NSIs support differentiating mixture plumes from multiple versus single source scenarios (see section Processing asynchronous odor mixtures)?

bioRxiv preprint doi: https://doi.org/10.1101/2020.07.23.217216; this version posted July 24, 2020. The copyright holder for this preprint (which was not certified by peer review) is the author/funder, who has granted bioRxiv a license to display the preprint in perpetuity. It is made available under a CC-BY 4.0 International License.

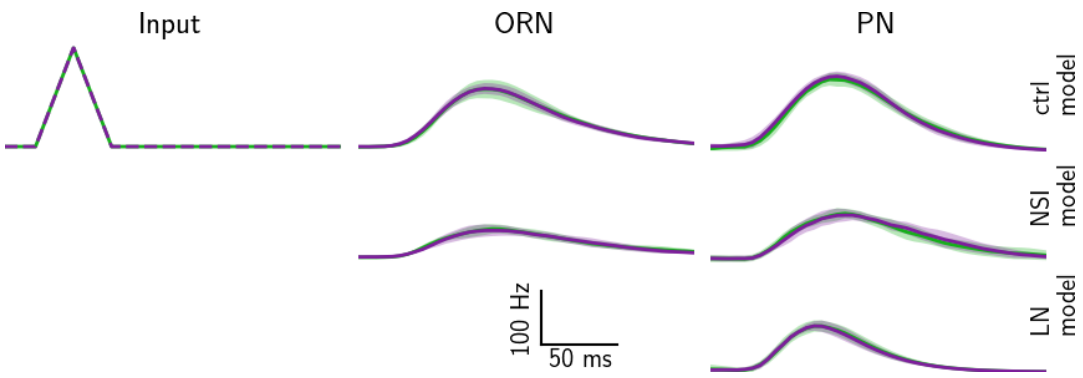

Figure 5. Time course of ORN (2nd column), and PN activity (3rd column) in response to a triangular pulse (50 ms, 1st column) for the three models – control (top row), NSI (second row) and LN model (bottom row). Green and purple lines are for glomerulus a and b, respectively. Input to the three models is identical, while control and LN models have identical ORN activity, which is therefore not displayed twice. Peak PN activity for the control-model is around 110 Hz (top row), and around 70 Hz for the NSI- and LN models. The lines show the average response and the shaded area around the lines the standard deviation over 10 trials.

Odorant ratio in synchronous mixture stimuli

Airborne odors travel in complex plumes characterized by highly intermittent whiffs and highly variable odor concentration (***Mylne and Mason, 1991***; ***Yee et al., 1995***). To successfully navigate such plumes and find for example food, flies must recognize relevant whiffs regardless of the overall odor concentration in them, i.e. perform concentration-independent odorant ratio recognition. This is a difficult problem as 1. PN responses are sigmoidal with respect to concentration and 2. the sigmoids are not the same for different odorants in a mixture and different receptor types. To investigate this problem and understand whether NSIs may play a role in solving it, we stimulated the model ORNs with binary mixtures, varying the overall concentration of the mixture, the concentration ratio, and the onset time of the two odorants. As a first approximation we mimic the whiffs in plumes (see e.g. ***Figure 6–Figure Supplement 2***a) with simple triangular odorant concentration profiles that have a symmetric linear increase and decrease (see ***Figure 5***). We first analysed the synchronous case where both odorants in the mixture arrive at the same time, which is typical when a single source emits both odorants (see ***Figure 7–Figure Supplement 1*** a, extracted from ***Erskine*** (***2018***)). To assess the role of NSIs, we compared the model with NSIs ("NSI model") to a model with lateral inhibition between PNs mediated by LNs in the AL ("LN model") and a control model where the pathways for different OR types do not interact at all ("control model").

Figure 5 shows the typical effects of the two mechanisms on PN responses. For the purpose of this figure we adjusted the NSI strength and LN synaptic conductance (see Table 1) in such a way that the average PN responses to a synchronous mixture pulse were matched across the two models. While the stimulus lasts only 50 ms, the effect on ORNs, PNs and LNs lasts more than twice as long. We observed the same behavior for other stimulus durations (tested from 10 to 500 ms). In the control model (***Figure 5***, top row), PN and LN responses are unaffected by lateral interactions between OR-type specific pathways and because we have matched the sensory response strength of the two odorants and OR types for simplicity, the responses of the PN in the two glomeruli are very much the same. For the LN model the response of ORNs is unaltered by network effects and synaptic inhibition of LNs is the only lateral interaction between pathways (***Figure 5*** bottom). For the NSI model (***Figure 5*** middle row) ORN activity is directly affected by NSIs and the activity of PNs is lower than in control conditions as a consequence of the lower ORN responses. As explained above, NSI strength and synaptic conductance of LN inhibition were chosen in this example so that the response of the PNs for both models is of similar magnitude (peak response for PNs for independent glomeruli ∼110Hz, for AL lateral inhibition and NSI mechanism ∼70 Hz).

To investigate the effectiveness of the two mechanisms for ensuring faithful odorant ratio en-

bioRxiv preprint doi: https://doi.org/10.1101/2020.07.23.217216; this version posted July 24, 2020. The copyright holder for this preprint (which was not certified by peer review) is the author/funder, who has granted bioRxiv a license to display the preprint in perpetuity. It is made available under a CC-BY 4.0 International license.

coding more systematically, we tested the three models with synchronous triangular odor pulses of different overall concentration, different concentration ratios, and for different values of stimulus duration (from 10 to $200\,\mathrm{ms}$), which we selected to match the range of common whiff durations observed experimentally (see ***Figure 6–Figure Supplement 2***). Here, and throughout the study we explored several values for the two strength parameters (1, 2, 3, 6,10, 13, 16 for ω_{NSI} and (0.2, 0.3, 0.4 for α_{LN}) and for each analysed task we report the results of the best performing NSI and LN model, respectively.

The results are summarised in ***Figure 6***. Due to the fundamentally sigmoidal PN responses for increasing odorant concentration (see ***Figure 4***e), the encoding of the ratio between two odorants in a mixture is distorted in the absence of additional mechanisms (as seen in the control model, ***Figure 6***a,b. The encoding of odorant mixtures is indeed already disrupted at the level of the ORNs (***Figure 6***a), not only on the level of PNs (***Figure 6***b). Once activated, inhibitory interactions between PNs mediated by LNs improve ratio encoding (***Figure 6***c,d) but only for a very limited range of stimulus concentrations: Essentially only for the concentration 0.6, the response ratio of PNs reasonably follows the diagonal. For other concentration values, LN inhibition is either too strong (diverging response ratio) or too weak (flat response ratio). We explored a wide range of values for α_{LN}, the synaptic efficacy of LN to PN synapses, and found that different values of α_{LN} lead to successful ratio encoding for different individual concentration values but that the overall qualitative behavior was unchanged. In other words, stronger or weaker LN inhibition does not improve ratio encoding in PN activity across more than one input concentration value. The NSI mechanism instead changes the ORN responses (***Figure 6***e), and as a consequence, PN responses change so that their activity reflects the ratio of odor concentrations better for most of the tested concentration ratios (***Figure 6***f).

The results in ***Figure 6*** are all based on the ratio of peak activity $R^{PN} = \nu_b^{PN}/\nu_a^{PN}$ (see Model and methods) during the first 100ms after the stimulus onset. We also tested the ratio of average activity over the duration of the stimuli and found very similar results (see ***Figure 6–Figure Supplement 1***). In the same vein, testing with longer stimuli also yielded qualitatively similar results.

Next, we tested the encoding of ratios – besides for different concentrations – also for different whiff durations (***Figure 6***g). For very short stimuli ($10\,\mathrm{ms}$), the sigmoidal dependence of PN responses on concentration does not yet have pronounced effects, and therefore ratio encoding is easier in the control model. However, the LN model over-compensates, leading to errors for all concentrations. In the NSI model the coding is as good as in control. For short stimuli ($20\,\mathrm{ms}$), the encoding in the control model begins to degrade, while the LN model improves for larger concentrations. The NSI model does best across all concentrations. For medium to very long stimuli ($50\,\mathrm{ms}$,$100\,\mathrm{ms}$) encoding in the LN model begins to break down again for larger concentrations while the NSI model exhibits constant coding quality. While very intuitive, encoding mixture ratios linearly in PN firing rates is not the only option. To analyse encoding quality more generally, we therefore repeated our analysis by calculating the mutual information (MI) between the odorant concentration and R^{PN}. The results from the analysis of the MI are qualitatively similar to the results with the coding error (see ***Figure 6–Figure Supplement 3***).

From this analysis it is evident that both NSI and AL inhibition lead to better ratio encoding than the control model for medium to long stimuli of high concentration. However, for the LN model this comes at the price of degraded ratio encoding at shorter stimulus durations and lower concentrations. Only the NSI model, albeit not perfect, improves ratio encoding consistently across all tested combinations for duration and concentration.

In the next section we will explore the effectiveness of the different models when the whiffs arrive asynchronously.

Processing asynchronous odor mixtures

When odorants are released from separate sources, they form a plume in which the whiffs of different odorants typically are encountered at distinct onset times. To the contrary, when a mixture

bioRxiv preprint doi: https://doi.org/10.1101/2020.07.23.217216; this version posted July 24, 2020. The copyright holder for this preprint (which was not certified by peer review) is the author/funder, who has granted bioRxiv a license to display the preprint in perpetuity. It is made available under a CC-BY 4.0 International License.

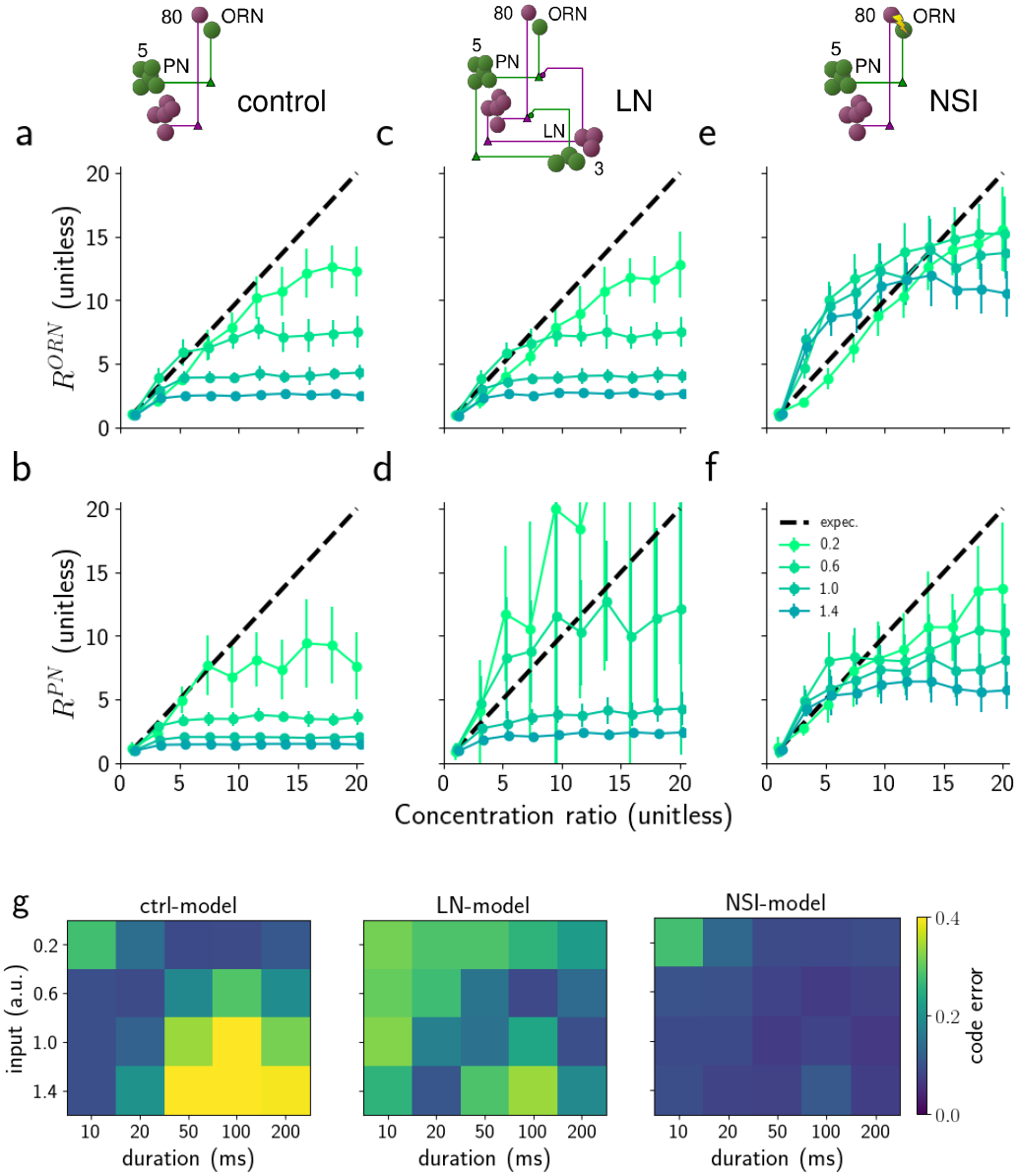

Figure 6. Encoding concentration ratio with peak PN activity. ORN (a,c,e) and PN (b,d,f) responses ratio ($R^{ORN} = v_b^{ORN}/v_a^{ORN}$ and $R^{PN} = v_b^{PN}/v_a^{PN}$) to a single synchronous triangular pulse of 50 ms duration applied to both ORN groups. The graphs show response ratios versus concentration ratio of the two odorants for four different overall concentrations (colours, see legend in f). The peak PN responses would be a perfect reflection of the odorant concentration if they followed the black dashed diagonal for all concentrations. Error bars represent the semi inter-quartile range calculated over 50 trials. g) Analysis of the coding error for different values of stimulus duration (from 10 to 200ms) and concentration values (0.2 to 1.4). The coding error is calculated as the squared relative distance (see Model and methods).

Figure 6–Figure supplement 1. Encoding ratio with the average PN activity.

Figure 6–Figure supplement 2. Plume statistics of natural plumes.

Figure 6–Figure supplement 3. Encoding ratio analysis with MI.

bioRxiv preprint doi: https://doi.org/10.1101/2020.07.23.217216; this version posted July 24, 2020. The copyright holder for this preprint (which was not certified by peer review) is the author/funder, who has granted bioRxiv a license to display the preprint in perpetuity. It is made available under a CC-BY 4.0 International license.

of odorants is released from a single source they form a plume where the odorants typically arrive together (***Figure 7–Figure Supplement 1***). We hypothesise that if lateral inhibition (via LNs or NSIs) only takes effect in the synchronous case but not in asynchronous case, it will help distinguishing single source and multi-source plumes. For instance, in the case of pheromone receptor neurons that are co-housed with receptor neurons for an antagonist odorant, the response to the pheromone would be suppressed by NSI when both odorants arrive in synchrony (same source) and not when arriving with delays (the pheromone source is separate from the antagonistic source). This is thought to underlie the ability of male moths to identify a compatible female, where the antagonist odorant is a component of the pheromone of a related but incompatible species ***Baker et al.*** (***1998***). To test whether this idea is consistent with the effect of NSIs as described by our model, we calculated the predicted responses of PNs to asynchronous whiffs of two odorants in our three models - *control, with LN inhibition, and with NSI*.

Figure 7a shows the responses in the models for the example of two $50\,\mathrm{ms}$ triangular odor pulses of the same amplitude and at $100\,\mathrm{ms}$ delay. We chose stimuli that excite the two ORN types with the same strength to simplify the analysis and focus on the differences between models with respect to asynchronous input rather than differing input ratios that we analyzed above. In the control model, responses are very similar between ORN_a and ORN_b, as well as, PN_a and PN_b as expected in the absence of interactions and for identical stimulus strength.

The situation is very different when LN inhibition is present (***Figure 7***a, bottom). Even for the comparatively large delay of $100\,\mathrm{ms}$ – the second stimulus starts $50\,\mathrm{ms}$ after the first one ends – the excitatory input to PN_b (purple) cannot overcome the inhibition coming through the LNs activated by PN_a (green). This is a consequence of PN and LN responses outlasting the stimuli as observed above. In contrast, while an inhibitory effect is present in the NSI model, it is much weaker, with only small effects at the PNs (***Figure 7***, middle row).

To quantify the differences between the three models across different typical conditions, we calculated the ratio between the PN responses of the two glomeruli $R^{PN} = \nu_b^{PN}/\nu_a^{PN}$, both for the peak activity and for the average activity over the stimulation time. ***Figure 7***b shows the results for stimulus durations between 10 and $200\,\mathrm{ms}$ and delays from 0 to $500\,\mathrm{ms}$. The whiff durations and delays were selected to match the range of values commonly observed in experiments (see ***Figure 6–Figure Supplement 2***).

As expected, the value of R^{PN} is close to 1 (pink lines) for the control model with independent ORNs and PNs and all explored parameters. In contrast, the NSI model and the LN model exhibit clear effects of their lateral interactions. In the LN model the response of the second PN_b is strongly suppressed by the response to the first stimulus for all tested whiff durations and delays. The NSI model also shows suppression but the effects are smaller and only present for very long whiffs ($200\,\mathrm{ms}$) and commensurate or shorter delays ($<250\,\mathrm{ms}$). This is a clear advantage over the LN model. The results are very similar whether measured in terms of the peak activity (***Figure 7***b) or the average activity over the stimulus duration (***Figure 7–Figure Supplement 2***).

Correlation detection in long realistic plumes

So far we have seen that NSIs are beneficial for ratio coding in synchronous mixtures and that they distort responses less than LN inhibition in the case of asynchronous mixtures. In this final section, we investigated and compared the effects of the two mechanisms when the system is stimulated with more realistic signals of fluctuating concentrations that have statistical features resembling odor plumes in an open field (see ***Figure 6–Figure Supplement 2***). The statistics of the plumes and how we simulated them are described in detail in the Model and methods; in brief, we replicated the statistical distribution of the duration of whiffs and clean air and the distribution of the odorant concentration which were reported in the literature (***Mylne and Mason, 1991***; ***Yee et al., 1995***). Similarly to ***Jacob et al.*** (***2017***), we simulated plumes as pairs of odorant concentration time series, with a varying degree of correlation to emulate plumes of odors emitted from a single or from two separate sources (see ***Erskine*** (***2018***) and ***Figure 7–Figure Supplement 1***). Similar to the

bioRxiv preprint doi: https://doi.org/10.1101/2020.07.23.217216; this version posted July 24, 2020. The copyright holder for this preprint (which was not certified by peer review) is the author/funder, who has granted bioRxiv a license to display the preprint in perpetuity. It is made available under a CC-BY 4.0 International license.

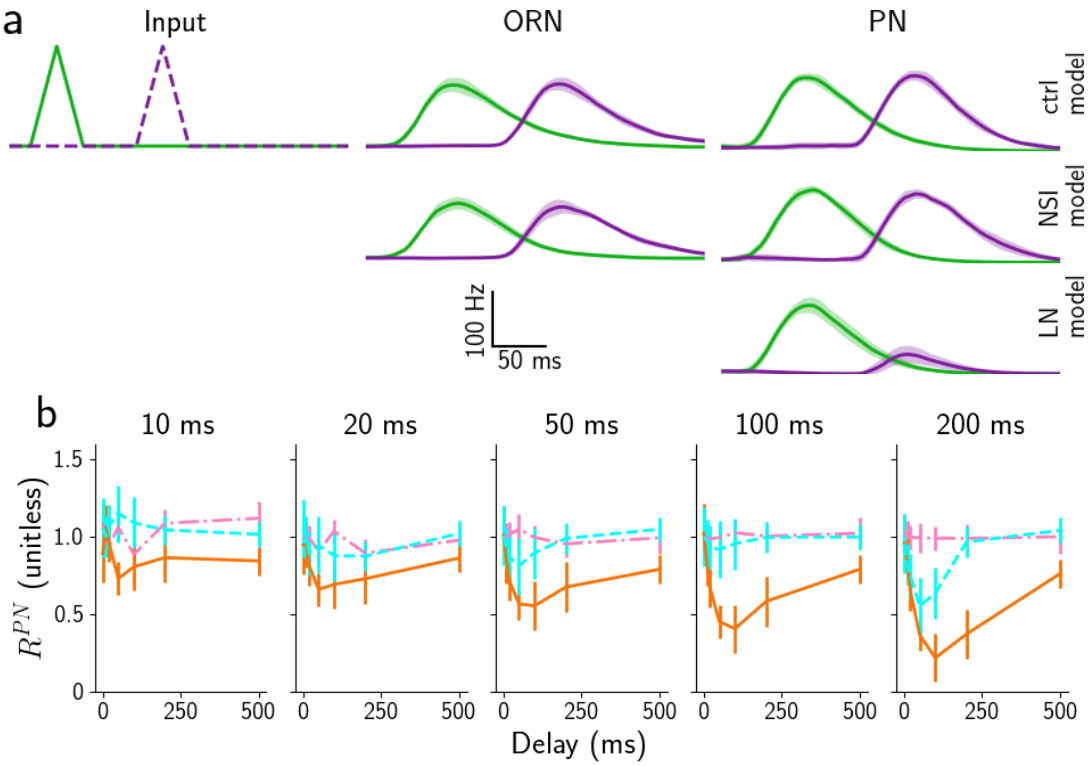

Figure 7. Asynchronous mixture encoding. a) Stimulus concentration ("Input", first column), and the response of ORNs (second column) and PNs (third column). The lines are the average response, and the shaded areas mark the standard deviation calculated over 10 trials. The PN peak activity for the control-model (top row) is ~150Hz for both glomeruli, for the LN model (bottom row) ~50Hz for the second glomerulus and for the NSI model (middle row) ~130 Hz for the second glomerulus. b) Median ratio of the peak PN responses of the two glomeruli $R^{PN} = v_b^{PN}/v_a^{PN}$ in the three models: control model (dot dashed pink), LN model (orange continuous), and NSI model (dashed cyan) for different stimulus durations as marked on the top. Error bars represent the semi inter-quartile ranges.

Figure 7–Figure supplement 1. Example concentration fluctuation time series for two odorants emitted by a single source or two separate sources

Figure 7–Figure supplement 2. Results for the average PN response over the stimulus duration.

bioRxiv preprint doi: https://doi.org/10.1101/2020.07.23.217216; this version posted July 24, 2020. The copyright holder for this preprint (which was not certified by peer review) is the author/funder, who has granted bioRxiv a license to display the preprint in perpetuity. It is made available under a CC-BY 4.0 International license.

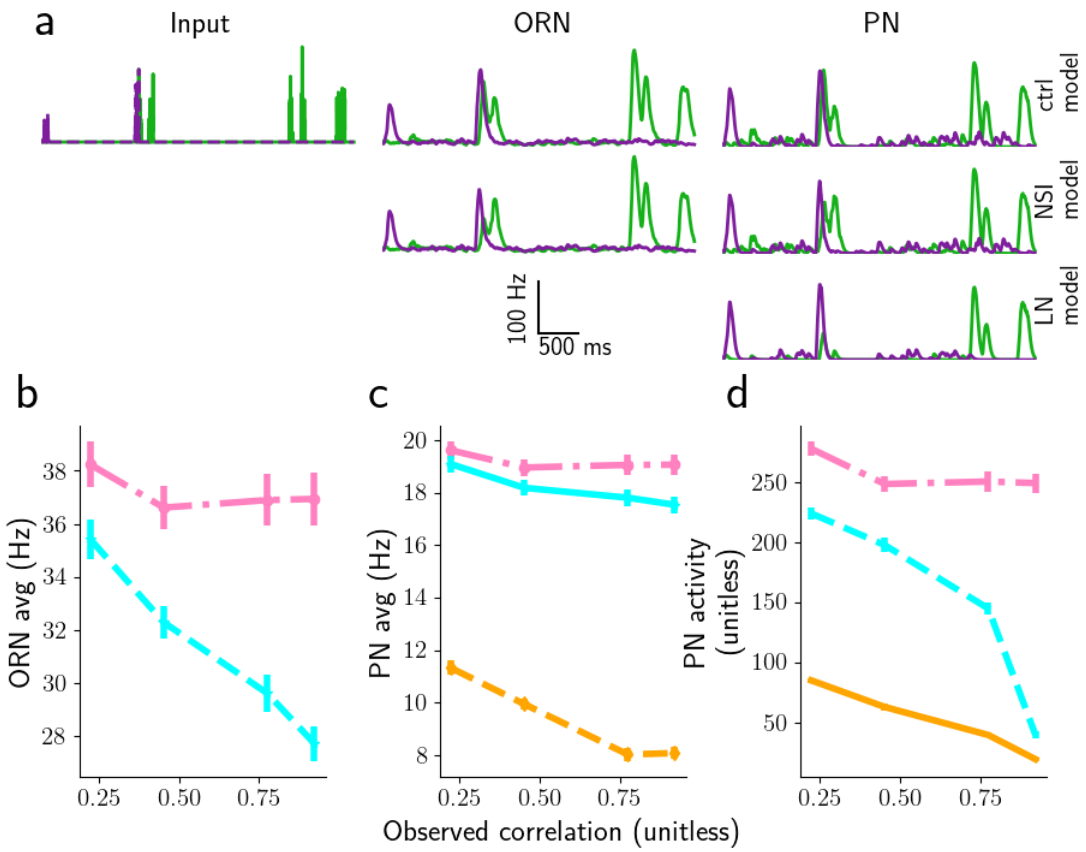

Figure 8. a) Time course of stimulus concentration (Input ORN, first column), and response of ORNs (second column), PNs (third column) to two 4 s long realistic plumes with statistical properties as described in the text; first row: control model, second row: NSI model, third row: LN model. Lines are the mean and shaded areas around the lines the standard deviation over 10 trials. b) Response of ORNs, and c) response of PNs averaged over 200 s for the three models: control model (dot dashed pink), LN model (orange continuous), and NSI model (dashed cyan). The observation from the LN model is not shown in panel b as it overlaps with the dot dashed pink lines (ctrl-model). d) Total PN activity above 150 Hz, for 3 ms maximum whiff durations.

Figure 8–Figure supplement 1. Statistical properties of simulated natural plumes

Figure 8–Figure supplement 2. Similar results of panel d with different thresholds (50, 100, 150 Hz)

previous section, the stimuli were applied to the models and we analyzed the PN responses in order to understand the ability of the early olfactory system to encode the signal. PN responses are very complex time series (see ***Figure 8***) and many different decoding algorithms (***Huerta et al., 2004***; ***Nowotny et al., 2005***; ***Jortner et al., 2007***; ***Lin et al., 2007***, ***2014***), could be present in higher brain areas to interpret them. However, as before, we applied the simple measure of peak PN activity in terms of the total firing rate above a given threshold to analyze the quality of the encoding.

In order to analyze the discrimination of plumes with odorants coming from a single source – highly correlated stimuli – from separate sources – poorly correlated stimuli – we developed a method to generate plumes of a prescribed correlation between concentration time series while keeping other properties such as intermittency and average odorant concentration constant (see Model and methods and ***Figure 8–Figure Supplement 1***). Using this method, we then explored plumes with correlation 0 to very close to 1. We simulated the model for 200 s duration (a few times the maximal timescale in plumes, i.e. 50 s) and preset correlations between the odorant concentration time series, and first inspected the average activity of neuron types over the stimulation period. By construction, the ORN activity for the LN model is the same as in the absence of inhibition (***Figure 8***a-b), while the average ORN activity for the NSI model is lower and depends on the correlation between odor signals (***Figure 8***a-b). These effects are approximately the same for the

bioRxiv preprint doi: https://doi.org/10.1101/2020.07.23.217216; this version posted July 24, 2020. The copyright holder for this preprint (which was not certified by peer review) is the author/funder, who has granted bioRxiv a license to display the preprint in perpetuity. It is made available under a CC-BY 4.0 International license.

whole range of the tested NSI strengths ω_{NSI} (data not shown).

The situation is different for the average PN activity. The average PN response in the NSI model is almost the same as in the control model and only weakly, if at all, dependent on input correlation (see ***Figure 8***c). It, therefore, does not encode input correlation well. To the contrary, the average PN responses in the LN inhibition network are lower than in the control model, and a bit more clearly dependent on input correlation (***Figure 8***c). Hence, LN inhibition is useful for encoding input correlation with the average PN activity. All reported effects remain approximately the same for the entire range of explored parameters (ω_{NSI} and α_{LN}) (data not shown).

We next analysed instead of the average PN response the "peak PN" response, defined as the integrated PN activity over time windows where the PN firing rate is above a given threshold (e.g. 50, 100, or $150\,\mathrm{ms}$). ***Figure 8***d shows peak PN for $150\,\mathrm{Hz}$ threshold (see ***Figure 8–Figure Supplement 2*** for plots with other underlying thresholds). For the LN model and the NSI model, peak PN responses depend on the plume correlation. Within the values we investigated, the highest peak threshold of $150\,\mathrm{Hz}$ recovers the most information about input correlation and for high peak thresholds the NSI mechanism leads to more informative responses than than LN inhibition. We conclude that most of the information about input correlations is contained in the first part of the response before adaptation takes place and that therefore the average activity over the entire response is not a good proxy for encoding the correlations in the input signals.

So far we have used simulated plumes corresponding to $60\,\mathrm{m}$ distance from the source. At different distances the maximum whiff durations will vary (***Pannunzi and Nowotny, 2019***). We therefore asked whether and how the efficiency of the two mechanisms depends on maximum whiff duration and hence distance from the source. To address this question, we generated plumes with different maximum whiff duration, w_{max}. ***Figure 9***a shows a plot for each tested value of w_{max} (from 0.01 to $50\,\mathrm{m}$) for peak threshold $150\,\mathrm{Hz}$ (see ***Figure 9–Figure Supplement 1*** and ***Figure 9–Figure Supplement 2*** for results with peak thresholds of 50, and $100\,\mathrm{Hz}$). The choice of maximum whiff durations reflects typical experimental observations (***Yee et al., 1995***).

There are two effects that are evident: 1. At zero correlation between the stimuli, PN responses in the NSI model are quite similar to those in the control model while those in the LN model differ more, and 2. The PN responses in the NSI model depend more strongly on the input correlations of the stimuli than the PN activities in the LN model, especially for short (<3s) whiffs (***Figure 9***a) which constitute more than 90% of all typical whiff durations. This second effect is important because ideally we would like the PN responses to differ maximally between highly correlated plumes and independent plumes in order to discern the two conditions.

To quantify these effects we measured the following distances: 1. The distance between peak PN of the NSI model (or LN model) and of the control model at zero correlation, defined as $p^0_{ctrl} - p^0_x$ with $x \in$ (NSI,LN) (***Figure 9***b) and 2. the distance between peak PN of NSI model (or LN model) at 0 correlation and at correlation (very close to) 1, defined as $p^0_x - p^1_x$ with $x \in$ (NSI,LN) (***Figure 9***c). These figures show the clear advantage of using an NSI mechanism instead of LN inhibition when encoding the correlation between stimuli that resemble a naturalistic plume: $p^0_{ctrl} - p^0_{NSI}$ is always always smaller than $p^0_{ctrl} - p^0_{LN}$ and $p^0_x - p^1_{NSI}$ is consistently larger than $p^0_x - p^1_{LN}$.

Discussion

"Thought experiment is in any case a necessary precondition for physical experiment. Every experimenter and inventor must have the planned arrangement in his head before translating it into fact." E. Mach (1905)

We have implemented a model of the early olfactory system comprising ORNs of two receptor types, their NSIs in the sensillum, and two corresponding glomeruli in the AL, containing PNs and LNs in roughly the numbers that have been observed for *Drosophila*. Our objective was to investigate two potential roles of NSIs in insects' olfactory processing: Concentration invariant mixture ratio recognition, vital for insects to identify the type or state of an odor source (see e.g. ((***Visser***

bioRxiv preprint doi: https://doi.org/10.1101/2020.07.23.217216; this version posted July 24, 2020. The copyright holder for this preprint (which was not certified by peer review) is the author/funder, who has granted bioRxiv a license to display the preprint in perpetuity. It is made available under a CC-BY 4.0 International License.

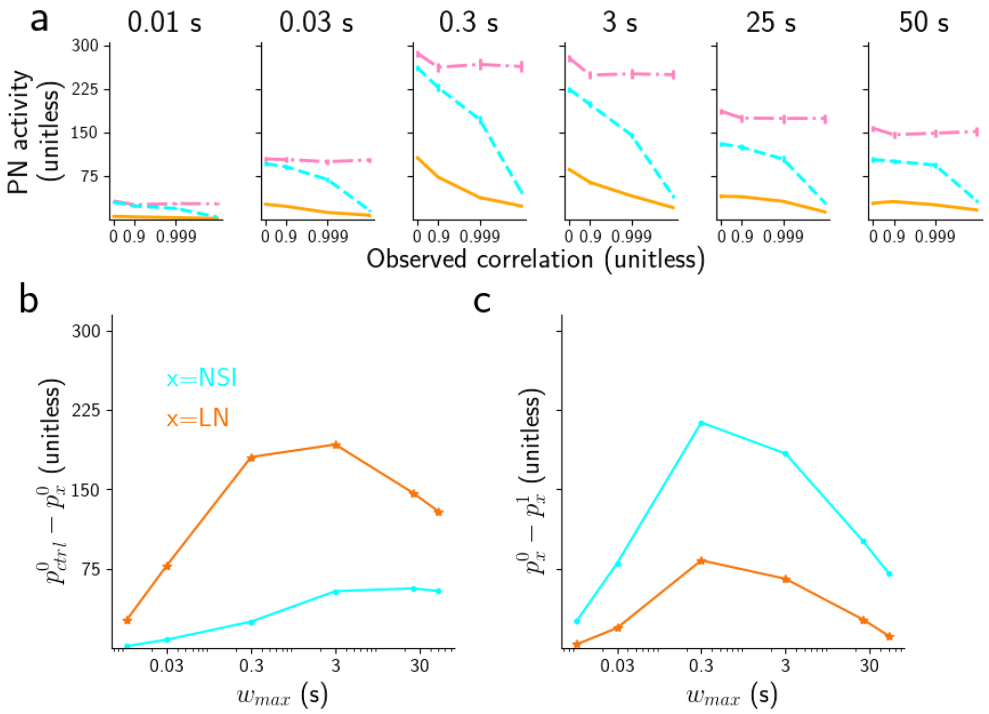

Figure 9. a) Peak PN for threshold $150\,\mathrm{Hz}$, and for different subsets of whiff durations (from 0.01 to 50s) for the three models: control model (dot dashed pink), LN model (orange continuous), and NSI model (dashed cyan). Note that the horizontal axis has a log-scale. b) Distance between the PN activity of the control model and the NSI model (or LN model), at 0 correlation, $p^0_{ctrl} - p^0_x$ with $x \in$ (NSI,LN). c) Distance between the PN activity of NSI model (or LN model) at 0 correlation and at correlation 1, $p^0_x - p^1_x$ with $x \in$ (NSI,LN).

Figure 9–Figure supplement 1. Similar results using threshold $50\,\mathrm{Hz}$

Figure 9–Figure supplement 2. Similar results using threshold $100\,\mathrm{Hz}$

bioRxiv preprint doi: https://doi.org/10.1101/2020.07.23.217216; this version posted July 24, 2020. The copyright holder for this preprint (which was not certified by peer review) is the author/funder, who has granted bioRxiv a license to display the preprint in perpetuity. It is made available under a CC-BY 4.0 International license.
Manuscript submitted to eLife

and Avé, 1978; *Christensen et al., 1989*; *Natale et al., 2003*; *Bruce et al., 2005*; *Najar-Rodriguez et al., 2010*) and references therein) and odor source separation, which can be critical for insects, e.g. in the context of finding mates *Baker et al.* (*1998*); *Fadamiro and Baker* (*1997*); *van Naters and Carlson* (*2007*). This second function requires high spatiotemporal resolution of odor recognition in complex plumes.

By comparing our model with NSIs to a control model without lateral interactions between pathways for different receptor types, we found evidence that NSIs should be beneficial for concentration invariant mixture processing: NSIs lead to more faithful representation of odor mixtures by PNs in the sense that the ratio of PN activity is closer to the ratio of input concentrations when NSIs are present. Similarly, the mutual information between the ratio of input concentrations and the ratio of PN activity is higher for the NSI model. While we admittedly do not know how exactly odor information is represented in PN activity, responses that differ systematically with input ratio must be superior to responses that saturate and hence do not inform about the input ratio, as seen in the control model.

Furthermore, using a model variant with no NSIs but LN inhibition between glomeruli in the AL we found that 1. For synchronous individual whiffs, both models, the one with NSI mechanism and the one with LN inhibition, are better than the control model in several conditions (*Figure 6* g); moreover, the NSI mechanism is typically more effective than LN inhibition. This is especially true for very short stimuli (<100ms). 2. For asynchronous individual whiffs, PN responses to the later whiff are strongly altered by the response to the first whiff when LN inhibition is present. In contrast, with NSIs the PN responses to the second whiffs are only mildly affected by the activity triggered by the first whiff, indicating that with NSIs there is less of a trade-off between benefits in encoding synchronous mixtures and distortions when odorants from separate sources mix.

These results further support the hypothesis that the NSI mechanism offers an evolutionary advantage by enabling more precise odor coding for these simple stimuli. Similar conclusions can be drawn when analyzing the capacity of the insect olfactory systems to encode the correlation between two odorants in a more realistic setting of an odor plume. We found that, when analysing peak PN activity (the integrated PN firing rate over windows during which it is above a given threshold), the model with NSI mechanism outperforms the LN inhibition model and both are better when considering peak activity than when considering average PN activity. Besides supporting the benefits of NSIs this also adds further evidence in favor of using peak activity to encode important features of a signal, in this case stimulus correlations, as hypothesized in earlier work (see e.g. *Krofczik et al.* (*2009*); *Wilson et al.* (*2017*)).

The model and its limitations

"A good model should not copy reality, it should help to explain it", *Segev* (*1992*).

As in every modelling work the level of description must match the purpose of the investigation. In terms of Marr's categorisation of models (*Marr and Poggio, 1976*), our model is somewhere between the algorithmic level - as both our models implement a form of lateral inhibition - and the implementation level - albeit we are not yet able to capture the underlying physics of the NSI mechanism. Because of our hypotheses that the role of NSIs is to improve processing of temporally complex stimuli, we focused on a description which included temporal dynamics but was otherwise as simple as possible. We therefore have simplified 1. the cellular dynamics of odor transduction (*Kaissling, 2001*, *2009*, *2014*, *2019*; *Gu and Rospars, 2011*; *Gorur-Shandilya et al., 2017*) and only heuristically describe the macroscopic effects at the receptor neuron level, an approach similar to (*Lazar and Yeh, 2020*); 2. the complexity of the full receptor repertoire in the insect olfactory system, e.g. about 60 ORN types in *Drosophila*, and instead focused on a single sensillum with two co-housed ORNs; 3. the true complexity of the many different LN types and transmitters in the AL (*Silbering et al., 2008*), using only $GABA_A$-like LNs. 4. the spatial distribution of the sensilla on the surface of the antenna or the maxillary palp; 5. the complexity of odor stimuli delivered by stimulation devices in the experiments we are mimicking for the single pulse investigation (see the

bioRxiv preprint doi: https://doi.org/10.1101/2020.07.23.217216; this version posted July 24, 2020. The copyright holder for this preprint (which was not certified by peer review) is the author/funder, who has granted bioRxiv a license to display the preprint in perpetuity. It is made available under a CC-BY 4.0 International license.

corresponding Model and methods section, (***Pannunzi and Nowotny, 2019***)), 6. the asymmetry of NSIs where there is some evidence that the strength of the NSIs is proportional to the size of the ORN that is exerting the interaction onto another neuron ***Zhang et al.*** (***2019***). By making these simplifications we were able to reduce the number of free parameters in the model, reasonably constrain most parameters and scan the few remaining parameters, such as the strength of LN inhibition, across a reasonable range. This increases our confidence that the observed benefits of NSIs for olfactory information processing are not artefacts of particular parameter choices in the model(s).

For the sake of simplicity we chose to work with a specific animal model in mind and because of the large amount of information available in the literature, we chose *Drosophila*. It will be interesting to see whether and how much our results can be generalized to other insect such as bees, mosquitoes or moths.

Comparison with related modelling works

"If I have seen further it is by standing on the shoulders of Giants." I. Newton (1675).

Our work builds on ideas in previous models (e.g., ***Chan et al.*** (***2018***); ***Rospars et al.*** (***2008***); ***Vermeulen and Rospars*** (***2004***)) and concurrent approaches (e.g. ***Lazar and Yeh*** (***2020***)). While earlier modeling works focused on the oscillatory and patterned dynamics of activity in the antennal lobe (***Bazhenov et al., 2001a***,b; ***Linster et al., 1993***; ***Linster and Smith, 1997***; ***Linster et al., 2005***), it was soon realized that the recognition of odorants and their mixtures across different concentrations posed a particularly difficult question. One school of models explored the idea of winnerless competition as a dynamical systems paradigm for concentration invariant coding (***Laurent et al., 2001***; ***Kwok, 2007***) while others explored more direct gain control mechanism mediated by local neurons in the AL (***Getz and Lutz, 1999***; ***Schmuker et al., 2011***; ***Serrano et al., 2013***). The task becomes even more difficult when the exact ratio of mixtures needs to be recognised, and a network model for mixture ratio detection for very selective pheromone receptors has been formulated in (***Zavada et al., 2011***). However, generally, odors already interact at the level of individual ORs due to competitive and non-competitive mechanisms which can be recapitulated in models, see e.g. (***Rospars et al., 2008***) for vertebrates and (***Chan et al., 2018***) for invertebrates.

However, our model also makes a clear departure from the large number of models that have been built on assumptions and data based on long, essentially constant, odor step stimuli. While these kind of stimuli are not impossible, they can be considered as the exception more than the rule; for instance, even at more than $60\,\mathrm{m}$ from the source, around 90% of whiffs last less than $200\,\mathrm{ms}$ (***Justus et al., 2002***; ***Yee et al., 1993***), see (***Pannunzi and Nowotny, 2019***) for review. This insight is particularly difficult to reconcile with models that emphasize and depend on intrinsically generated oscillations in the antennal lobe (***Bazhenov et al., 2001a***,b; ***Linster et al., 2005***, ***1993***; ***Linster and Smith, 1997***), and models that depend on comparatively slow, intrinsically generated dynamics such as the models based on the winnerless competition mechanism (***Rabinovich et al., 2001***; ***Laurent et al., 2001***). The original interpretation of these models, how they use intrinsic neural dynamics to process essentially constant stimuli, is disrupted when stimuli have their own fast dynamics. How to reconcile the idea of intrinsic neural dynamics for information processing with natural odor stimuli that have very rich temporal dynamics of their own remains an open problem.

In building our model, we followed the main ideas developed by ***Vermeulen and Rospars*** (***2004***) but went beyond the assumption of constant stimuli and also added the important element of adaptation in ORNs and PNs, a widely accepted feature that is important in the context of dynamic stimuli; and while ***Vermeulen and Rospars*** (***2004***) already were interested in possible evolutionary advantages of NSIs, we here added the comparison with lateral inhibition in the AL that has been described as a competing mechanism, from an experimental (e.g. ***Todd and Baker*** (***1999***)) and a theoretical point of view (e.g., ***Getz and Lutz*** (***1999***); ***Zavada et al.*** (***2011***); ***Serrano et al.*** (***2013***). Finally an important addition in this study are the mixture stimuli: Many, though not all, earlier

bioRxiv preprint doi: https://doi.org/10.1101/2020.07.23.217216; this version posted July 24, 2020. The copyright holder for this preprint (which was not certified by peer review) is the author/funder, who has granted bioRxiv a license to display the preprint in perpetuity. It is made available under a CC-BY 4.0 International License.

works focused on the response of the network to mono-molecular odors, whereas we analyse the network response to two-odorant mixtures.

A previous study with very similar motivation relating to mixture ratio recognition is the analysis of pheromone ratio recognition of ***Zavada et al.*** (***2011***). However, this earlier work still assumed constant stimuli, no adaptation in ORNs, a fixed target input ratio and only LN inhibition.

Further hypotheses about NSIs

"there is always a well-known solution to every human problem—neat, plausible, and wrong." H. L. Mencken 1920 "Prejudices: Second Series"

At this early stage, our knowledge and underdstanding of NSIs is still full of gaps. For example, while suggestive our results cannot prove beyond doubt whether NSIs are effectively useful to the olfactory system, or if they are an evolutionary spandrel. We also do not know their evolutionary history. One interesting idea would be that the complex function of improved odor mixture encoding could have arisen as a side effect from a simpler function, e.g. of saving space, but we do not have any evidence to support this.

Researchers in the past 20 years have suggested a number of non exclusive explanations for the functions of NSIs. We have analyzed two of them - improved odor ratio representation and detecting plume correlations. Other typical hypotheses are: 1. NSIs may be useful to generally enhance the dynamic range of ORN responses. Based on an electrical circuit model ***Vermeulen and Rospars*** (***2004***) showed an increased dynamic range of responses in the more strongly activated ORN in a sensillum. While the model does not include established experimental insights, e.g. ORN adaptation ***Kim et al.*** (***2011***); ***Martelli et al.*** (***2013***), its main assumptions remain plausible. 2. NSIs could facilitate novelty detection for odor signals on the background of other odors ***Todd and Baker*** (***1999***), if newly arriving "foreground odors" suppress the ongoing response to an already present "background odor".

The improvement of dynamic range by NSIs sits alongside work that showed that syntopic interactions at the receptor level and masking interactions at a cellular level achieve similar effects ***Reddy et al.*** (***2018***); ***Singh et al.*** (***2019***) as well as improving mixture representations. Similarly, ***Chan et al.*** (***2018***) showed that syntopic interactions improve concentration invariant mixture representation in particular for odors with many components. How these receptor-level and cell-level mechanisms interact with sensillum-level NSIs is an interesting future research question.

With regards to separating foreground odors from background odors, ***Todd and Baker*** (***1999***) noticed early on that NSIs duplicate the role of LNs in the AL even though (***Wilson, 2013***) pointed out later that LN networks take effect later and mainly decorrelate PN activities and normalize them with respect to the *average input* from ORNs. Here we have added to the discussion by showing that NSIs have advantages with respect to their faster timescale that led to less disruption of asynchronous odor whiffs.

Moreover, NSIs have two additional key advantages with respect to LN inhibition in the AL or processes in later brain areas: 1. NSIs take effect without the need to generate spikes and reduce the number of necessary spikes which makes them energetically advantageous (***Hasenstaub et al., 2010***; ***Laughlin, 2001***, ***1998***; ***Lennie, 2003***; ***Sarpeshkar, 1998***). 2. NSIs take place at the level of the single sensillum and hence a few spikes and synapses earlier than any AL or later interactions (***Todd and Baker, 1999***; ***Wilson, 2013***). In the AL the information from ORNs of the same type is likely pooled and information about the activity of individual ORNs is not retained (see e.g. ***Kazama and Wilson*** (***2009***); ***Nagel and Wilson*** (***2011***)). Therefore, while interactions within the sensillum are precise in space and time, interactions in the AL will be global (averaged over input from many sensilla) and information channels will interact in an averaged fashion. Similar local interactions in the very early stages of sensory perception were already discussed for the retina (***Klaassen et al., 2016***; ***Thoreson and Mangel, 2012***).

bioRxiv preprint doi: https://doi.org/10.1101/2020.07.23.217216; this version posted July 24, 2020. The copyright holder for this preprint (which was not certified by peer review) is the author/funder, who has granted bioRxiv a license to display the preprint in perpetuity. It is made available under a CC-BY 4.0 International License.

Conclusions

In conclusion, we have demonstrated in a model of the early olfactory system that NSIs have advantages over LN inhibition in the AL with respect to faithful mixture ratio recognition and plume separation. In our future work we seek to confirm the behavioral relevance of NSIs in *Drosophila*. Other interesting future directions include the relationship of NSIs and syntopic effects/masking, as well as the differential roles of NSIs and LN inhibition when both are present at the same time.

Model and methods

Model topology

We model the electrical activity of the early olfactory system of *Drosophila melanogaster*. The model encompasses ORNs on the antenna, and the matching glomeruli in the AL, containing PNs and LNs. For simplicity, ORNs are housed in sensilla in pairs, and each neuron in a pair expresses a different OR type. The paired neurons interact through NSIs, effectively leading to mutual inhibition (see ***Figure 1*** a). There are multiple sensilla of the same type on each antenna. We here model 40 sensilla per type (***Kazama and Wilson, 2009***). ORNs of the same type all project exclusively to the same glomerulus in the AL, making excitatory synapses onto the associated PNs. In addition to the inputs from ORNs, PNs also receive global excitation from PNs associated with other glomeruli and from other parts of the brain. They are inhibited by the LNs of other glomeruli but not by LN in the same glomerulus (see ***Figure 2***). The model simulates one type of sensillum and hence two types of ORNs, ORN_a and ORN_b. We assume that ORN_a and ORN_b are selectively activated by odorants A and B, respectively (see ***Figure 2*** and ***Figure 1*** a).

Olfactory Receptor Neurons

We describe ORN activity in terms of an odorant transduction process combined with a biophysical spike generator (***Lazar and Yeh, 2020***). During transduction, odorants bind and unbind at olfactory receptors according to simple rate equations. As we are not interested in the competition of different odorants for the same receptors, we simplify the customary two-stages binding and activation model (***Rospars et al., 2008***; ***Nowotny et al., 2013***; ***Chan et al., 2018***) to a single binding rate equation for the fraction r of receptors bound to an odorant,

$$\dot{r} = b_r C^n (1 - r) - d_r r \tag{2}$$

$$\begin{aligned} \dot{x} &= a_x r - c_x y(1 + d_x x) - b_x x \\ \dot{y} &= a_y x - b_y y \end{aligned} \tag{3}$$

where x is the 'activation' of the ORN and y an internal adaptation variable. The firing ν of the ORN is then obtained by a sigmoid filter applied to x,

$$\nu = \frac{\nu_{max}}{1 + exp(-a_{rect}(x - c_{rect}))} \tag{4}$$

The parameters (a_x, b_x, a_r, c_x, d_y, b_y) are rate constants that are estimated together with b_r and d_r to reproduce the data presented in ***Lazar and Yeh*** (***2020***); ***Martelli et al.*** (***2013***). The maximum spike rate ν_{max} and sigmoid shape parameters a_{rect} and c_{rect} are given in 1. The model is similar in nature to the models presented in (***De Palo et al., 2013***; ***Lazar and Yeh, 2020***) albeit simplified and formulated in more tangible rate equations. As we will demonstrate below, this simplified model can reproduce experimental data equally well as the previous models. In order to simulate the spiking output of a population of ORNs of a given type, we simulate the odor binding dynamics once to obtain the firing rate ν and then sample from $N_{ORN} = 40$ Poisson processes with rate ν. Using Poisson processes is very common for the sake of simplicity, and it is also close to experimental observations (see e.g. ***Kaissling*** (***2014***)). However, ORN firing of homotypic ipsi-lateral ORNs has been observed to have specific correlations (***Kazama and Wilson, 2009***) that are not automatically

bioRxiv preprint doi: https://doi.org/10.1101/2020.07.23.217216; this version posted July 24, 2020. The copyright holder for this preprint (which was not certified by peer review) is the author/funder, who has granted bioRxiv a license to display the preprint in perpetuity. It is made available under a CC-BY 4.0 International license.

reproduced by independent Poisson spike trains. To replicate the experimentally observed correlations - correlation for homotypic ipsi-lateral without stimulation around 0.14 and for homotypic ipsi-lateral under stimulation is around 0.2 - we extracted the random numbers for the generation of the Poissonian spike trains of the ORNs from a multivariate normal distribution with a covariance matrix of this shape: 1 in the diagonal, c_{hom} for the elements connecting homotypic neurons (see 1) and 0 all the others.

Non-synaptic interactions

To simulate experimentally observed NSIs, we assume a simple linear model with respect to the output variable of the transduction model, as the exact biochemical mechanism for NSIs is of yet unclear. We do this with a multiplicative term (x_a x_b) to reflect that presumably the driving force for x_a (x_b) is removed, rather than ORN_a (ORN_b) being directly hyperpolarized.

$$\begin{aligned} \dot{x}_a &= a_x r_a - c_x y_a (1 + d_x x_a) - b_x x_a - \omega_{\text{NSI}} x_a x_b \\ \dot{x}_b &= a_x r_b - c_x y_b (1 + d_x x_b) - b_x x_b - \omega_{\text{NSI}} x_a x_b \end{aligned} \tag{5}$$

The full set of parameters used for the simulations are reported in Table1.

The antennal lobe

We here reduce the antennal lobe (AL) to two glomeruli, a and b (see Fig. Topology) in order to focus on the effects of NSIs of the corresponding ORN types. The numbers of PNs and LNs per glomerulus are as reported in literature (***De Bruyne et al., 2001***; ***Kazama and Wilson, 2009***; ***Stocker, 1994***; ***Vosshall et al., 1999***).

The competing LNs are inhibitory whereas the PN is excitatory. For simplicity, we do not model multiple kinds of LNs or PNs that have been observed in the AL. Similar models are being used extensively in the analysis of the insect AL (***Chan et al., 2018***; ***Schmuker et al., 2011***; ***Serrano et al., 2013***; ***Zavada et al., 2011***) and are well suited for replicating the competition dynamics that we seek to evaluate.

Each ORN spike (width sp_{length} and height sp_{height}) from the N_{ORNs} is summed into a variable, u_{ORN}. PN and LN spikes have the same width sp_{length} and height sp_{height} and per each (impinging) neuron, PN or LN, they are summed into the variables u_{PN} and u_{LN}, respectively. u_{ORN} together with u_{LN} drives the activity of the corresponding PN:

$$\begin{aligned} \tau_{\text{V}} \dot{V} &= (V_{\text{rest}}^{\text{PN}} - V) + s\,(V_{\text{rev}}^{\text{PN}} - V) \\ \tau_s \dot{s} &= \alpha_{ORN} u_{\text{ORN}}\,(1 - s)\,(1 - x)\,(1 - y) - s \\ \tau_{\text{x}} \dot{x} &= \alpha_{\text{x}}\, u_{\text{ORN}}\,(1 - x) - x \\ \tau_{\text{y}} \dot{y} &= \alpha_{LN}\, u_{\text{LN}}\,(1 - y) - y \end{aligned} \tag{6}$$

where V is the PN membrane potential, s represents the combined action of synaptic inputs, x is an adaptation variable, and y is the inhibitory variable impinging into PNs. Each one of these variables has its time constant - τ_s, τ_V, τ_x, and τ_y. The multiplicative factors α_{LN}, α_{ORN} reflects the amount of released vesicles per each spike from an ORN and LN, respectively and they can be considered synaptic strength. In the second equation, the term (1-y) reflects the inhibition from LNs, implementing a pre-synaptic type of inhibition proportional to the low-pass filtered activity of the LNs. When V>Θ, the PN fires a spike and V is reset to V_{rest}.

LNs receive excitatory input from PNs and are otherwise described by a similar model but without adaptation,

$$\begin{aligned} \tau_V \dot{V} &= (V_{\text{rest}}^{\text{LN}} - V) + s\,(V_{\text{rev}}^{\text{LN}} - V) \\ \tau_{\text{s}} \dot{s} &= \alpha_{\text{PN}} u_{\text{PN}}\,(1 - s) - \beta_{\text{LN}} s \end{aligned} \tag{7}$$

where V is the LN membrane potential, s represents the synaptic input, and α_{PN} reflects the rate of transmitter release, or synaptic strength, for incoming synapses from a PN. When V>Θ, the LN fires a spike and V is reset to V_{rest}. The refractory period, τ_{ref}, for PNs and LNs lasts 2 ms. All the parameters used for the simulations are reported in 1. The comparative analysis between the LN

bioRxiv preprint doi: https://doi.org/10.1101/2020.07.23.217216; this version posted July 24, 2020. The copyright holder for this preprint (which was not certified by peer review) is the author/funder, who has granted bioRxiv a license to display the preprint in perpetuity. It is made available under a CC-BY 4.0 International license.

inhibition and NSI mechanism has been carried out through the exploration of the two parameters α_{LN} and the strength of the NSIs, ω_{NSI}.

Odor stimuli

To compare the model response with the neurophysiological results in the literature and with previous models (***Lazar and Yeh, 2020***), we analyzed its activity with different stimuli: step stimuli, u_{step}, ramp stimuli u_{ramp} and parabolic stimuli u_{par}.

$$u_{\text{step}}(t) = \begin{cases} c, & t_1 \le t \le t_2 \\ 0, & \text{otherwise} \end{cases} \tag{8}$$

$$u_{par}(t) = \begin{cases} c(\frac{t-t_1}{t_2-t_1-\delta})^2, & t_1 \le t \le t_2 - \delta \\ c(1 - \frac{t-t_2+\delta}{\delta})^2, & t_2 - \delta \le t \le t_2 \\ 0, & \text{otherwise.} \end{cases} \tag{9}$$

$$u_{\text{ramp}}(t) = \begin{cases} c\frac{t-t_1}{t_2-t_1-2\delta}, & t_1 \le t \le t_2 - 2\delta \\ c\left(1 - \frac{t-t_2+2\delta}{2\delta}\right), & t_2 - 2\delta \le t \le t_2 \\ 0, & \text{otherwise} \end{cases} \tag{10}$$

where t1= 0.5s, t2=2.5s, and δ= 0.1s (see ***Figure 3–Figure Supplement 1***).

Table 1. Model parameters. To fit the experimental data, we used the following 38 parameters: Transduction (3), ORNs (10), ORNs, PNs and LNs (18), and Network (7) parameters. We fitted ORN, PN and LN parameters in order to reproduce the time course shown in e-phys experiments (e.g. ***Kim et al.*** (***2011***); ***Martelli et al.*** (***2013***)); we fit the correlation parameters to obtain similar correlated values as those reported in (***Kazama and Wilson, 2009***); Network parameters are not fitted, but extracted from the literature (e.g. (***Kazama and Wilson, 2009***; ***Stocker, 1994***; ***Vosshall et al., 1999***)). NSI strength and synaptic strength of LNs are not fitted, but their values were changed to explore the network behavior.

Transduction		
n	1	
b_r	0.01	
d_r	0.009	

ORNs		
a_y	0.25	
b_y	0.002	
c_x	0.0028	
b_x	0.2	
d_x	1	
a_x	1	
ω_{NSI}	0.2	

Rectification function		
c_{rect}	1	
a_{rect}	3.3	
ν_{max}	250	Hz

Network		
$N_{orn,pn}$	18	
$N_{orn,glo}$	40	
$N_{pn,glo}$	5	
$N_{ln,glo}$	3	
N_{glo}	2	
c_{hom}	0.4	
$\nu_{pn,noise}$	250	Hz

LN, ORN, and PN		
τ_s	10	ms
τ_V	0.5	ms
sp_{length}	4	ms
Θ	1	
sp_{height}	0.3	Θ
τ_{ref}	2	ms

LNs		
V_{rest}^{LN}	-3	mV
V_{rev}^{LN}	15	mV
α_{LN}	10	
τ_y	600	ms
α_{PN}	2.5	
y_{LN0}	0.025	

PNs		
α_{ORN}	2.5	
V_{rest}^{PN}	-6.5	mV
V_{rev}^{PN}	15	mV
α_x	2	
τ_x	600	ms
x_{PN0}	0.48	

bioRxiv preprint doi: https://doi.org/10.1101/2020.07.23.217216; this version posted July 24, 2020. The copyright holder for this preprint (which was not certified by peer review) is the author/funder, who has granted bioRxiv a license to display the preprint in perpetuity. It is made available under a CC-BY 4.0 International License.

Simulation of realistic plumes

In a realistic scenario, odorants are mixed together in complex plumes that follow the laws of fluid dynamics. For these conditions, even odorants coming from different sources are sometimes mixed together, and one difficult task for insects is to recognize when two intermingled odorants are coming from the same source or from separate sources. Of course it is not possible to distinguish these two possibilities from a single, instantaneous sampling, but on average the odorants coming from the same source are more correlated than odorants coming from separate sources (see panel a of ***Figure 7–Figure Supplement 1***). To test the function of NSIs for odor source separation, we adopted long stimuli (>3 s), with statistical properties that resemble the filaments observed downwind from an odor source in an open environment (***Mylne and Mason, 1991***; ***Pannunzi and Nowotny, 2019***; ***Yee et al., 1993***, ***1995***) at zero crosswind distance. For these conditions, the distributions of whiff and clean air durations follow a power law with exponent -3/2 (see, e.g., ***Yee et al. (1993)***), and the cumulative distribution function (CDF) for the normalized concentration values will follow an exponential distribution and we fitted the CDF as a piecewise linear function, as follows

$$CDF(x) = \begin{cases} 5/3x, & 0 \le x \le 0.3 \\ (1 - 10^{-(a_1 + b_1 x)}), & \text{otherwise} \end{cases} \tag{11}$$

where x is the normalized concentration $C/\overline{C}$, and a1 and b1 are free parameters, which values were determined by fitting and are reported below in 1 (***Mylne and Mason, 1991***). We analysed stimuli with different 'intermittency factor', defined here as the proportion of time where odor concentration is non-zero (even though there are different definitions in use). To simulate the arrival of plumes of two odors with the aforementioned properties, we need to generate a time series of whiffs and blanks with the correct statistics for each odorant (like in (***Jacob et al., 2017***)) and the correct correlation between odorants. We achieved this by the following procedure:

1. We drew two correlated pseudo random numbers from a Gaussian distribution, with a given correlation
2. We mapped the two numbers into two uniform random variables
3. The uniform random variables are mapped into the desired power law distributions; blank and whiff durations have different distributions depending on the distance from the source (see ***Figure 6–Figure Supplement 2***).

Analysis and simulation

We used the PNs spiking activity as the output of the networks and we analysed it to estimate the ability of the three networks to encode odorants mixture ratio and spatio-temporal analysis. We assumed for simplicity that the relevant information is present in the firing rate and therefore analyse the average activity and peak activity, defined below and in the main text.

For the analysis of the ratio encoding (see ***Figure 6***), The concentration ratio is ratio between the weak and the strong concentration values, $R_c = c_w/c_s$; while the PN ratio is $R_\nu = \nu_w/\nu_s$.

We defined the coding error as the square relative distance between the ratio of the PN activity and the ratio of the odorant concentrations. The relative distance is therefore: $((R_c - R_\nu)/(R_c + R_\nu))^2$.

Spike density function Firing rates were obtained from the convolution of the spike trains with the kernel: $k(\hat{t}) = \hat{t}\, exp(-\hat{t}/\tau)$. Where $\hat{t} = t - t_{spike} + \tau$, so that the maximum of k is situated at the occurrence of the spike, t_{spike}. The timescale of the kernel was chosen as τ=20 ms (***Nawrot et al., 1999***).

The model was simulated with custom Python code, as well as the analysis of the simulations. All code is publicly available on github, https://github.com/mariopan/flynose.

Acknowledgments

The research in this paper has received funding from the Human Frontiers Science Program, Grant RGP0053/2015 (odor objects project), the European Union's Horizon 2020 research and innova-

bioRxiv preprint doi: https://doi.org/10.1101/2020.07.23.217216; this version posted July 24, 2020. The copyright holder for this preprint (which was not certified by peer review) is the author/funder, who has granted bioRxiv a license to display the preprint in perpetuity. It is made available under a CC-BY 4.0 International license.

tion program under Grant Agreement No. 785907 (HBP SGA2) and a Leverhulme Trust Research Project.

References

Andersson MN, Larsson MC, Blaženec M, Jakuš R, Zhang QH, Schlyter F. Peripheral modulation of pheromone response by inhibitory host compound in a beetle. Journal of Experimental Biology. 2010; 213(19):3332–3339.

Av-Ron E, Rospars JP. Modeling insect olfactory neuron signaling by a network utilizing disinhibition. Biosystems. 1995; 36(2):101–108.

Av-Ron E, Vibert JF. A model for temporal and intensity coding in insect olfaction by a network of inhibitory neurons. Biosystems. 1996; 39(3):241–250.

Baker TC, Fadamiro H, Cosse A. Moth uses fine tuning for odour resolution. Nature. 1998; 393(6685):530–530.

Bazhenov M, Stopfer M, Rabinovich M, Abarbanel HD, Sejnowski TJ, Laurent G. Model of cellular and network mechanisms for odor-evoked temporal patterning in the locust antennal lobe. Neuron. 2001; 30(2):569–581.

Bazhenov M, Stopfer M, Rabinovich M, Huerta R, Abarbanel HD, Sejnowski TJ, Laurent G. Model of transient oscillatory synchronization in the locust antennal lobe. Neuron. 2001; 30(2):553–567.

Binyameen M, Jankuvová J, Blaženec M, Jakuš R, Song L, Schlyter F, Andersson MN. Co-localization of insect olfactory sensory cells improves the discrimination of closely separated odour sources. Functional ecology. 2014; 28(5):1216–1223.

Bruce TJ, Wadhams LJ, Woodcock CM. Insect host location: a volatile situation. Trends in plant science. 2005; 10(6):269–274.

Chan HK, Hersperger F, Marachlian E, Smith BH, Locatelli F, Szyszka P, Nowotny T. Odorant mixtures elicit less variable and faster responses than pure odorants. PLoS computational biology. 2018; 14(12):e1006536.

Christensen TA, Mustaparta H, Hilderbrand JG. Discrimination of sex pheromone blends in the olfactory system of the moth. Chemical Senses. 1989; 14(3):463–477.

Couto A, Alenius M, Dickson BJ. Molecular, anatomical, and functional organization of the Drosophila olfactory system. Current Biology. 2005; 15(17):1535–1547.

De Bruyne M, Foster K, Carlson JR. Odor coding in the Drosophila antenna. Neuron. 2001; 30(2):537–552.

De Palo G, Facchetti G, Mazzolini M, Menini A, Torre V, Altafini C. Common dynamical features of sensory adaptation in photoreceptors and olfactory sensory neurons. Scientific reports. 2013; 3:1251.

Erskine A. Perception and representation of temporally patterned odour stimuli in the mammalian olfactory bulb. PhD thesis, University College London; 2018.

Fadamiro HY, Baker TC. Helicoverpa zea males (Lepidoptera: Noctuidae) respond to the intermittent fine structure of their sex pheromone plume and an antagonist in a flight tunnel. Physiological Entomology. 1997; 22(4):316–324.

Getz WM, Lutz A. A neural network model of general olfactory coding in the insect antennal lobe. Chemical senses. 1999; 24(4):351–372.

Gorur-Shandilya S, Demir M, Long J, Clark DA, Emonet T. Olfactory receptor neurons use gain control and complementary kinetics to encode intermittent odorant stimuli. Elife. 2017; 6:e27670.

Gu Y, Rospars JP. Dynamical modeling of the moth pheromone-sensitive olfactory receptor neuron within its sensillar environment. PLoS One. 2011; 6(3).

Hasenstaub A, Otte S, Callaway E, Sejnowski TJ. Metabolic cost as a unifying principle governing neuronal biophysics. Proceedings of the National Academy of Sciences. 2010; 107(27):12329–12334.

Huerta R, Nowotny T, García-Sanchez M, Abarbanel HD, Rabinovich MI. Learning classification in the olfactory system of insects. Neural computation. 2004; 16(8):1601–1640.

Jacob V, Monsempès C, Rospars JP, Masson JB, Lucas P. Olfactory coding in the turbulent realm. PLOS Computational Biology. 2017; 13(12):e1005870.

bioRxiv preprint doi: https://doi.org/10.1101/2020.07.23.217216; this version posted July 24, 2020. The copyright holder for this preprint (which was not certified by peer review) is the author/funder, who has granted bioRxiv a license to display the preprint in perpetuity. It is made available under a CC-BY 4.0 International License.

Jortner RA, Farivar SS, Laurent G. A Simple Connectivity Scheme for Sparse Coding in an Olfactory System. Journal of Neuroscience. 2007; 27(7):1659–1669. https://www.jneurosci.org/content/27/7/1659, doi: 10.1523/JNEUROSCI.4171-06.2007.

Justus KA, Murlis J, Jones C, Cardé RT. Measurement of odor-plume structure in a wind tunnel using a photoionization detector and a tracer gas. Environmental Fluid Mechanics. 2002; 2(1-2):115–142.

Kaissling KE. Olfactory perireceptor and receptor events in moths: a kinetic model. Chemical Senses. 2001; 26(2):125–150.

Kaissling KE. Olfactory perireceptor and receptor events in moths: a kinetic model revised. Journal of Comparative Physiology A. 2009; 195(10):895–922.

Kaissling KE. Pheromone reception in insects. The example of silk moths in Neurobiology of Chemical Communication. 2014; p. 99–146.

Kaissling KE. Responses of insect olfactory neurons to single pheromone molecules. In: *Olfactory Concepts of Insect Control-Alternative to Insecticides* Springer; 2019.p. 1–27.

Kazama H, Wilson RI. Origins of correlated activity in an olfactory circuit. Nature neuroscience. 2009; 12(9):1136.

Kim AJ, Lazar AA, Slutskiy YB. System identification of Drosophila olfactory sensory neurons. Journal of computational neuroscience. 2011; 30(1):143–161.

Kim AJ, Lazar AA, Slutskiy YB. Projection neurons in Drosophila antennal lobes signal the acceleration of odor concentrations. Elife. 2015; 4:e06651.

Klaassen LJ, de Graaff W, Van Asselt JB, Klooster J, Kamermans M. Specific connectivity between photoreceptors and horizontal cells in the zebrafish retina. Journal of neurophysiology. 2016; 116(6):2799–2814.

Krofczik S, Menzel R, Nawrot MP. Rapid odor processing in the honeybee antennal lobe network. Frontiers in computational neuroscience. 2009; 2:9.

Kwok YC. Encoding of odour blends in the moth antennal lobe. PhD thesis, University of Leicester; 2007.

Laughlin S. de Ruyter van Steveninck RR, Anderson JC. 1998. The metabolic cost of neural information Nat Neurosci. 1998; 1(36):10–1038.

Laughlin SB. Energy as a constraint on the coding and processing of sensory information. Current opinion in neurobiology. 2001; 11(4):475–480.

Laurent G, Stopfer M, Friedrich RW, Rabinovich MI, Volkovskii A, Abarbanel HD. Odor encoding as an active, dynamical process: experiments, computation, and theory. Annual review of neuroscience. 2001; 24(1):263–297.

Lazar AA, Yeh CH. A molecular odorant transduction model and the complexity of spatio-temporal encoding in the Drosophila antenna. PLOS Computational Biology. 2020; 16(4):e1007751.

Leal WS. Odorant reception in insects: roles of receptors, binding proteins, and degrading enzymes. Annual review of entomology. 2013; 58:373–391.

Lennie P. The cost of cortical computation. Current biology. 2003; 13(6):493–497.

Lin AC, Bygrave AM, de Calignon A, Lee T, Miesenböck G. Sparse, decorrelated odor coding in the mushroom body enhances learned odor discrimination. Nature Neuroscience. 2014; 17(4):559–568. https://doi.org/10.1038/nn.3660, doi: 10.1038/nn.3660.

Lin HH, Lai JSY, Chin AL, Chen YC, Chiang AS. A Map of Olfactory Representation in the Drosophila Mushroom Body. Cell. 2007; 128(6):1205 – 1217. http://www.sciencedirect.com/science/article/pii/S0092867407003170, doi: https://doi.org/10.1016/j.cell.2007.03.006.

Linster C, Masson C, Kerszberg M, Personnaz L, Dreyfus G. Formal model of the insect olfactory macroglomerulus. In: *Computation and Neural Systems* Springer; 1993.p. 255–259.

Linster C, Sachse S, Galizia CG. Computational modeling suggests that response properties rather than spatial position determine connectivity between olfactory glomeruli. Journal of neurophysiology. 2005; 93(6):3410–3417.

bioRxiv preprint doi: https://doi.org/10.1101/2020.07.23.217216; this version posted July 24, 2020. The copyright holder for this preprint (which was not certified by peer review) is the author/funder, who has granted bioRxiv a license to display the preprint in perpetuity. It is made available under a CC-BY 4.0 International license.

749 **Linster C**, Smith BH. A computational model of the response of honey bee antennal lobe circuitry to odor mix-
750 tures: overshadowing, blocking and unblocking can arise from lateral inhibition. Behavioural brain research.
751 1997; 87(1):1–14.

752 **Marr D**, Poggio T. From understanding computation to understanding neural circuitry. . 1976; .

753 **Martelli C**, Carlson JR, Emonet T. Intensity invariant dynamics and odor-specific latencies in olfactory receptor
754 neuron response. Journal of Neuroscience. 2013; 33(15):6285–6297.

755 **Mylne KR**, Mason P. Concentration fluctuation measurements in a dispersing plume at a range of up to 1000
756 m. Quarterly Journal of the Royal Meteorological Society. 1991; 117(497):177–206.

757 **Nagel KI**, Wilson RI. Biophysical mechanisms underlying olfactory receptor neuron dynamics. Nature neuro-
758 science. 2011; 14(2):208.

759 **Najar-Rodriguez AJ**, Galizia C, Stierle J, Dorn S. Behavioral and neurophysiological responses of an insect to
760 changing ratios of constituents in host plant-derived volatile mixtures. Journal of Experimental Biology. 2010;
761 213(19):3388–3397.

762 **Natale D**, Mattiacci L, Hern A, Pasqualini E, Dorn S. Response of female Cydia molesta (Lepidoptera: Tortricidae)
763 to plant derived volatiles. Bulletin of entomological research. 2003; 93(4):335–342.

764 **van Naters WvdG**, Carlson JR. Receptors and neurons for fly odors in Drosophila. Current biology. 2007;
765 17(7):606–612.

766 **Nawrot M**, Aertsen A, Rotter S. Single-trial estimation of neuronal firing rates: from single-neuron spike trains
767 to population activity. Journal of neuroscience methods. 1999; 94(1):81–92.

768 **Nowotny T**, Huerta R, Abarbanel HD, Rabinovich MI. Self-organization in the olfactory system: one shot odor
769 recognition in insects. Biological cybernetics. 2005; 93(6):436–446.

770 **Nowotny T**, Stierle JS, Galizia CG, Szyszka P. Data-driven honeybee antennal lobe model suggests how stimulus-
771 onset asynchrony can aid odour segregation. Brain research. 2013; 1536:119–134.

772 **Olsen SR**, Bhandawat V, Wilson RI. Divisive normalization in olfactory population codes. Neuron. 2010;
773 66(2):287–299.

774 **Pannunzi M**, Nowotny T. Odor stimuli: Not just chemical identity. Frontiers in Physiology. 2019; 10.

775 **Rabinovich M**, Volkovskii A, Lecanda P, Huerta R, Abarbanel H, Laurent G. Dynamical encoding by networks of
776 competing neuron groups: winnerless competition. Physical review letters. 2001; 87(6):068102.

777 **Reddy G**, Zak JD, Vergassola M, Murthy VN. Antagonism in olfactory receptor neurons and its implications for
778 the perception of odor mixtures. Elife. 2018; 7:e34958.

779 **Rospars JP**, Lansky P, Chaput M, Duchamp-Viret P. Competitive and noncompetitive odorant interactions in
780 the early neural coding of odorant mixtures. Journal of Neuroscience. 2008; 28(10):2659–2666.

781 **Sarpeshkar R**. Analog versus digital: extrapolating from electronics to neurobiology. Neural computation.
782 1998; 10(7):1601–1638.

783 **Schmuker M**, Yamagata N, Nawrot M, Menzel R. Parallel representation of stimulus identity and intensity in a
784 dual pathway model inspired by the olfactory system of the honeybee. Frontiers in neuroengineering. 2011;
785 4:17.

786 **Segev I**. Single neurone models: oversimple, complex and reduced. Trends in neurosciences. 1992; 15(11):414–
787 421.

788 **Serrano E**, Nowotny T, Levi R, Smith BH, Huerta R. Gain control network conditions in early sensory coding.
789 PLoS computational biology. 2013; 9(7).

790 **Shimizu K**, Stopfer M. Olfaction: intimate neuronal whispers. Nature. 2012; 492(7427):44–45.

791 **Silbering AF**, Okada R, Ito K, Galizia CG. Olfactory information processing in the Drosophila antennal lobe:
792 anything goes? Journal of Neuroscience. 2008; 28(49):13075–13087.

bioRxiv preprint doi: https://doi.org/10.1101/2020.07.23.217216; this version posted July 24, 2020. The copyright holder for this preprint (which was not certified by peer review) is the author/funder, who has granted bioRxiv a license to display the preprint in perpetuity. It is made available under a CC-BY 4.0 International License.
Manuscript submitted to eLife

793 **Singh V**, Murphy NR, Balasubramanian V, Mainland JD. Competitive binding predicts nonlinear responses
794 of olfactory receptors to complex mixtures. Proceedings of the National Academy of Sciences. 2019;
795 116(19):9598–9603.

796 **Stocker RF**. The organization of the chemosensory system in Drosophila melanogaster: a rewiew. Cell and
797 tissue research. 1994; 275(1):3–26.

798 **Su CY**, Menuz K, Reisert J, Carlson JR. Non-synaptic inhibition between grouped neurons in an olfactory circuit.
799 Nature. 2012; 492(7427):66–71.

800 **Szyszka P**, Stierle JS, Biergans S, Galizia CG. The speed of smell: odor-object segregation within milliseconds.
801 PloS one. 2012; 7(4).

802 **Thoreson WB**, Mangel SC. Lateral interactions in the outer retina. Progress in retinal and eye research. 2012;
803 31(5):407–441.

804 **Todd JL**, Baker TC. Function of peripheral olfactory organs. In: *Insect olfaction* Springer; 1999.p. 67–96.

805 **Vermeulen A**, Rospars JP. Why are insect olfactory receptor neurons grouped into sensilla? The teachings of a
806 model investigating the effects of the electrical interaction between neurons on the transepithelial potential
807 and the neuronal transmembrane potential. European Biophysics Journal. 2004; 33(7):633–643.

808 **Visser J**, Avé D. General green leaf volatiles in the olfactory orientation of the Colorado beetle, Leptinotarsa
809 decemlineata. Entomologia experimentalis et applicata. 1978; 24(3):738–749.

810 **Vosshall LB**, Amrein H, Morozov PS, Rzhetsky A, Axel R. A spatial map of olfactory receptor expression in the
811 Drosophila antenna. Cell. 1999; 96(5):725–736.

812 **Wilson CD**, Serrano GO, Koulakov AA, Rinberg D. A primacy code for odor identity. Nature communications.
813 2017; 8(1):1–10.

814 **Wilson RI**. Early olfactory processing in Drosophila: mechanisms and principles. Annual review of neuroscience.
815 2013; 36:217–241.

816 **Xu P**, Choo YM, Chen Z, Zeng F, Tan K, Chen TY, Cornel AJ, Liu N, Leal WS. Odorant inhibition in mosquito
817 olfaction. iScience. 2019; 19:25–38.

818 **Yee E**, Chan R, Kosteniuk P, Chandler G, Biltoft C, Bowers J. Measurements of level-crossing statistics of con-
819 centration fluctuations in plumes dispersing in the atmospheric surface layer. Boundary-layer meteorology.
820 1995; 73(1-2):53–90.

821 **Yee E**, Wilson D, Zelt B. Probability distributions of concentration fluctuations of a weakly diffusive passive
822 plume in a turbulent boundary layer. Boundary-Layer Meteorology. 1993; 64(4):321–354.

823 **Zavada A**, Buckley CL, Martinez D, Rospars JP, Nowotny T. Competition-based model of pheromone component
824 ratio detection in the moth. PloS one. 2011; 6(2).

825 **Zhang Y**, Tsang TK, Bushong EA, Chu LA, Chiang AS, Ellisman MH, Reingruber J, Su CY. Asymmetric ephaptic
826 inhibition between compartmentalized olfactory receptor neurons. Nature communications. 2019; 10(1):1–
827 16.

bioRxiv preprint doi: https://doi.org/10.1101/2020.07.23.217216; this version posted July 24, 2020. The copyright holder for this preprint (which was not certified by peer review) is the author/funder, who has granted bioRxiv a license to display the preprint in perpetuity. It is made available under a CC-BY 4.0 International license.

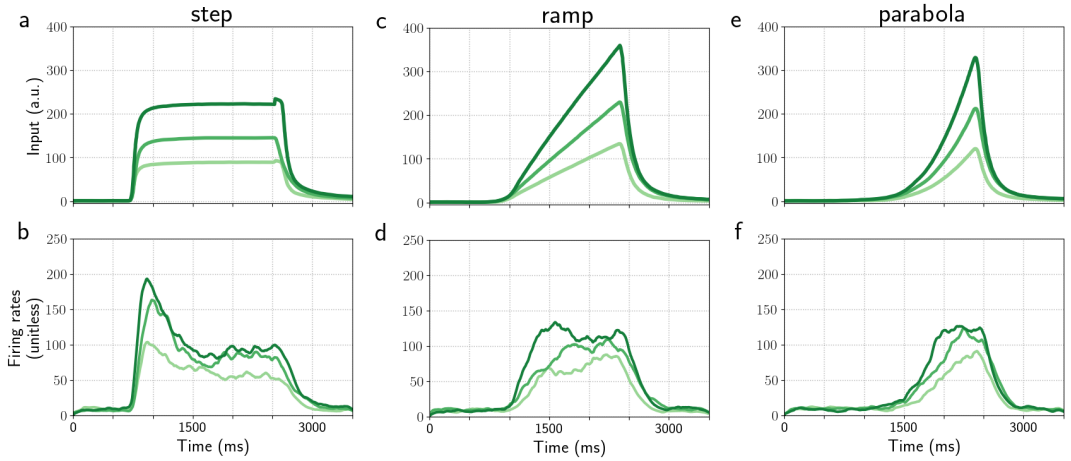

Figure 3–Figure supplement 1. Model ORN response to a single step (a,b), ramp (c,d), and parabola (e,f). a, c, e: Stimulus waveforms, i.e. odorant concentration profiles, as in ***Kim et al.*** (***2015***). b, d, f: Model ORN firing rates visualized as a spike density function (SDF).

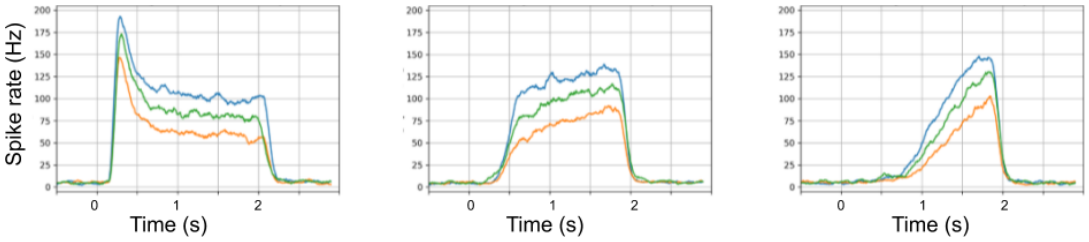

Figure 3–Figure supplement 2. Output of the model of Lazar and Yeh (***Lazar and Yeh, 2020***) for the Or59b receptor neuron in response to the corresponding stimulus waveforms (experimental data reported in ***Kim et al.*** (***2015***)).

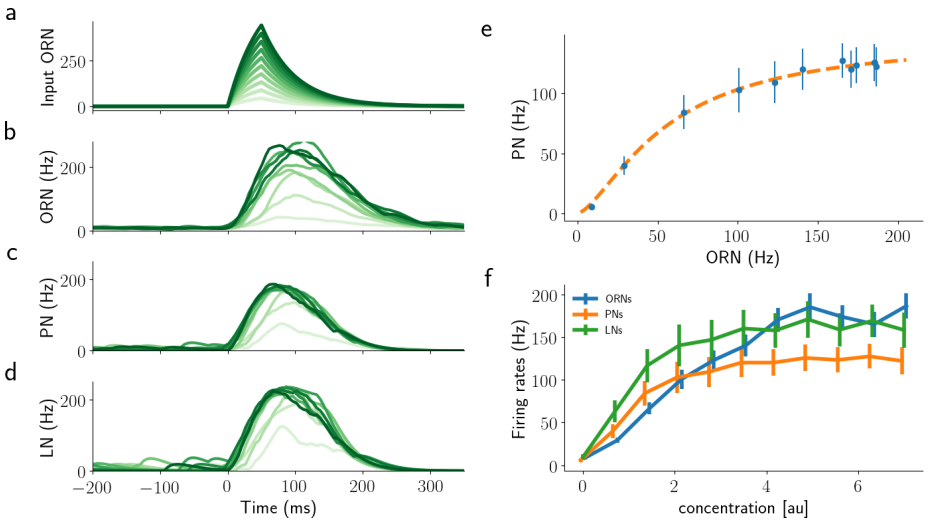

Figure 4–Figure supplement 1. a) 50 ms step stimuli, shade of green indicates concentration. b)-d) corresponding activity of ORNs, PNs, and LNs. Shades of green match the input concentrations. e) Average response of PNs over 50 ms against the average activity of the corresponding ORNs. The orange dashed line is the fit of the simulated data using equation eq.1 as reported in (***Olsen et al., 2010***). f) Average values for PNs, ORNs, and LNs for different values of concentration. Error bars show the SE over PNs.

bioRxiv preprint doi: https://doi.org/10.1101/2020.07.23.217216; this version posted July 24, 2020. The copyright holder for this preprint (which was not certified by peer review) is the author/funder, who has granted bioRxiv a license to display the preprint in perpetuity. It is made available under a CC-BY 4.0 International license.

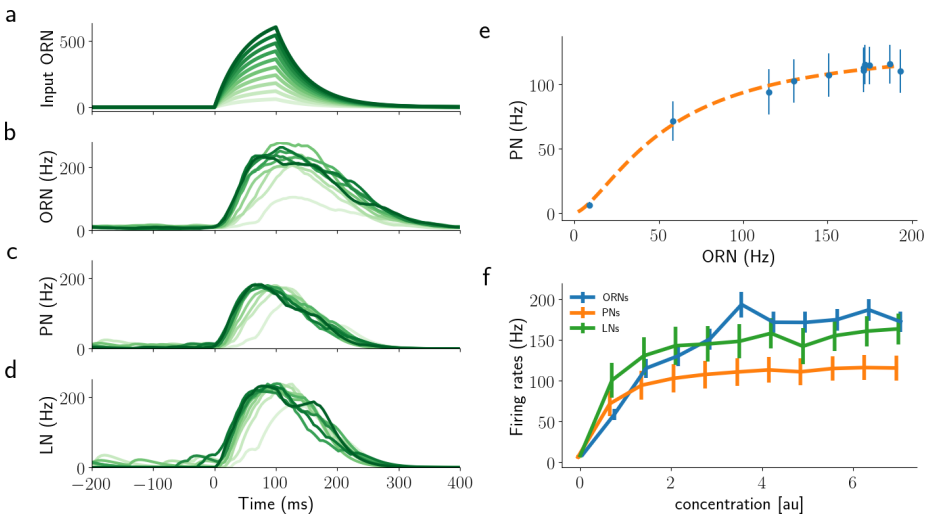

Figure 4–Figure supplement 2. a) 10 ms step stimuli, shade of green indicates concentration. b)-d) corresponding activity of ORNs, PNs, and LNs. Shades of green match the input concentrations. e) Average response of PNs over 10 ms against the average activity of the corresponding ORNs. The orange dashed line is the fit of the simulated data using equation eq.1 as reported in (***Olsen et al., 2010***). f) Average values for PNs, ORNs, and LNs for different values of concentration. Error bars show the SE over PNs.

bioRxiv preprint doi: https://doi.org/10.1101/2020.07.23.217216; this version posted July 24, 2020. The copyright holder for this preprint (which was not certified by peer review) is the author/funder, who has granted bioRxiv a license to display the preprint in perpetuity. It is made available under a CC-BY 4.0 International License.

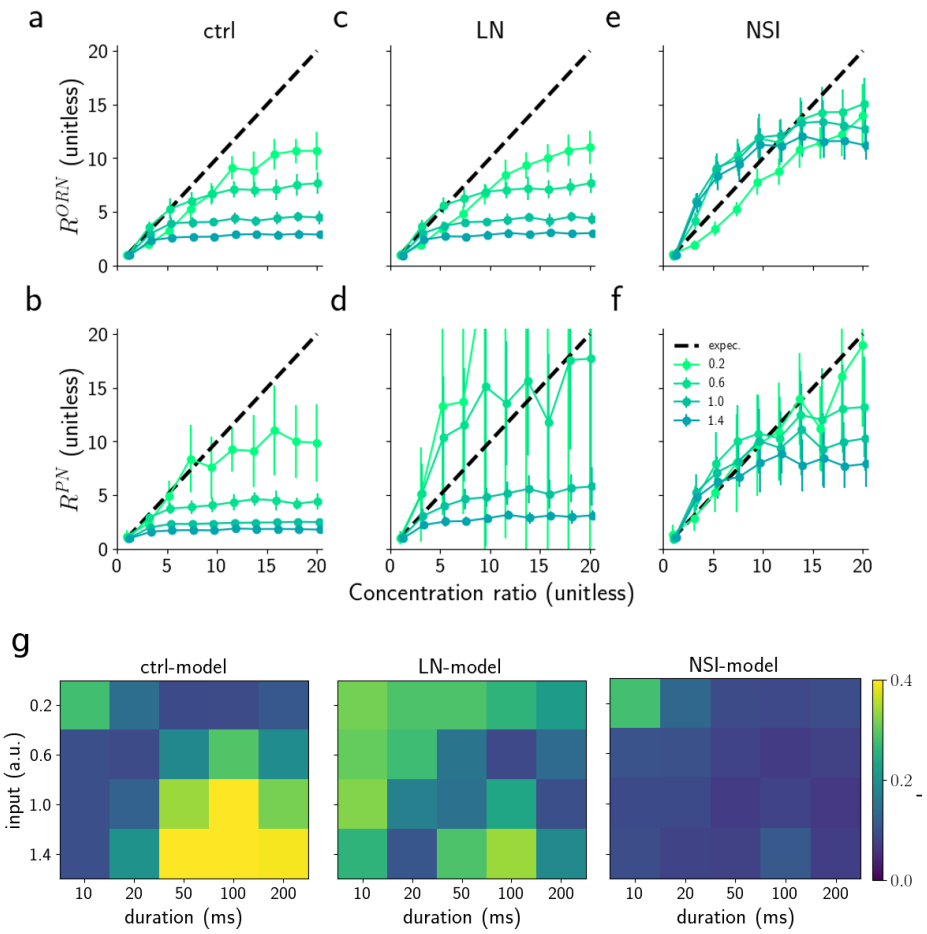

Figure 6–Figure supplement 1. Encoding ratio with the average PN activity. ORN (a,c,e) and PN (b,d,f) responses to a single synchronous triangular pulse of $50\,\mathrm{ms}$ duration applied to both ORN groups. The graphs show average responses ratio (R^{ORN} and R^{PN}), respectively, versus concentration ratio of the two odorants for four different overall concentrations (colours, see legend in f). The average PN responses would be a perfect reflection of the odorant concentration if they followed the black dashed diagonal for all concentrations. Error bars represent the semi inter-quartile range calculated over 50 trials. g) Analysis of the coding error for different values of stimulus duration (from 10 to 200ms) and concentration values (0.2 to 1.4).

bioRxiv preprint doi: https://doi.org/10.1101/2020.07.23.217216; this version posted July 24, 2020. The copyright holder for this preprint (which was not certified by peer review) is the author/funder, who has granted bioRxiv a license to display the preprint in perpetuity. It is made available under a CC-BY 4.0 International license.

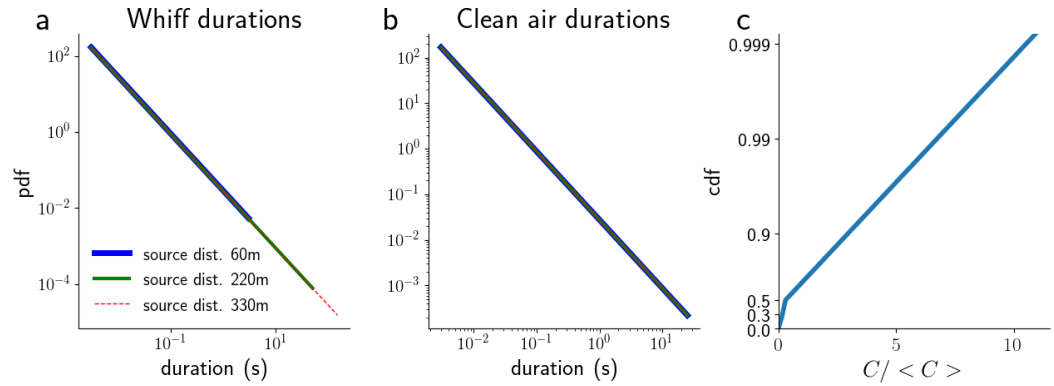

Figure 6–Figure supplement 2. a) Probability distribution of the whiff durations for odorants emitted at distances larger than $60\,\mathrm{m}$ ***Yee et al.*** (***1995***). b) Probability distribution of the blank durations for odorants emitted at distances larger than $60\,\mathrm{m}$ ***Yee et al.*** (***1995***). c) Probability distribution of the normalized concentration for odorants emitted at $75\,\mathrm{m}$ distance from the source ***Mylne and Mason*** (***1991***).

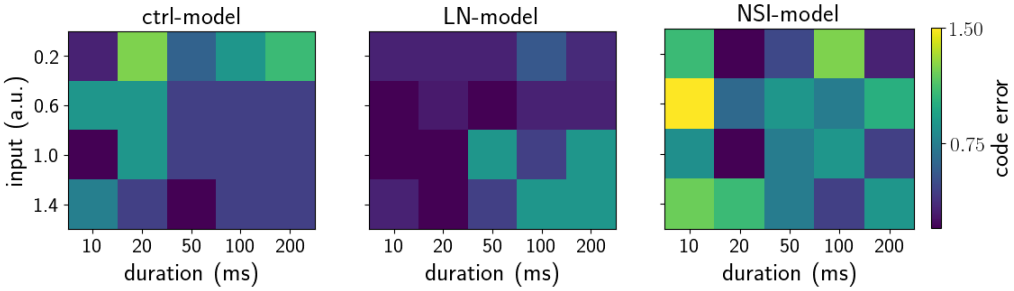

Figure 6–Figure supplement 3. Analysis of the coding error with mutual information for different values of stimulus duration (from 10 to 200ms) and concentration values (0.2 to 1.4). The coding error is calculated as the MI between odorant concentration and R^{PN} (see Model and methods).

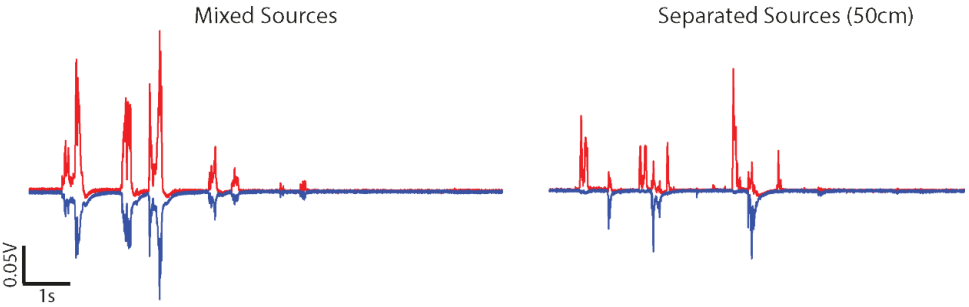

Figure 7–Figure supplement 1. Example concentration fluctuation time series of natural plumes for two odorants emitted by a single source or two separate sources (***Erskine, 2018***).

bioRxiv preprint doi: https://doi.org/10.1101/2020.07.23.217216; this version posted July 24, 2020. The copyright holder for this preprint (which was not certified by peer review) is the author/funder, who has granted bioRxiv a license to display the preprint in perpetuity. It is made available under a CC-BY 4.0 International License.

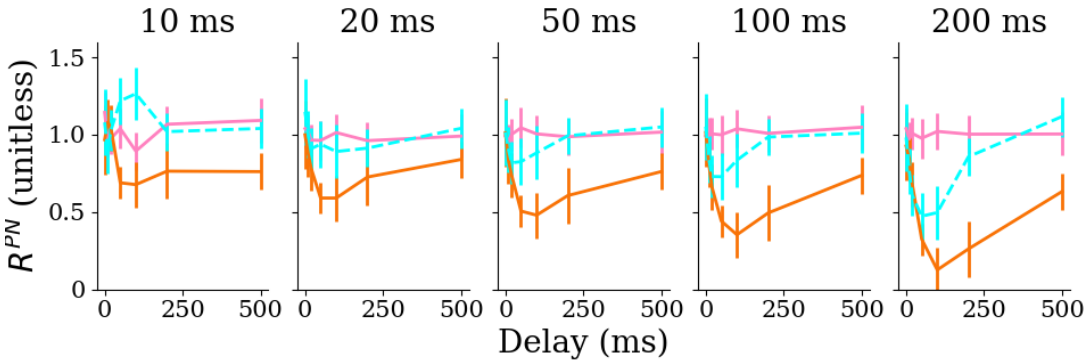

Figure 7–Figure supplement 2. Median ratio of the average PN responses of the two glomeruli $R^{PN} = v_b^{PN}/v_a^{PN}$ in the three models: control model (dot dashed pink), LN model (orange continuous), and NSI model (dashed cyan) for different stimulus durations as marked on the top. Error bars represent the semi inter-quartile ranges.

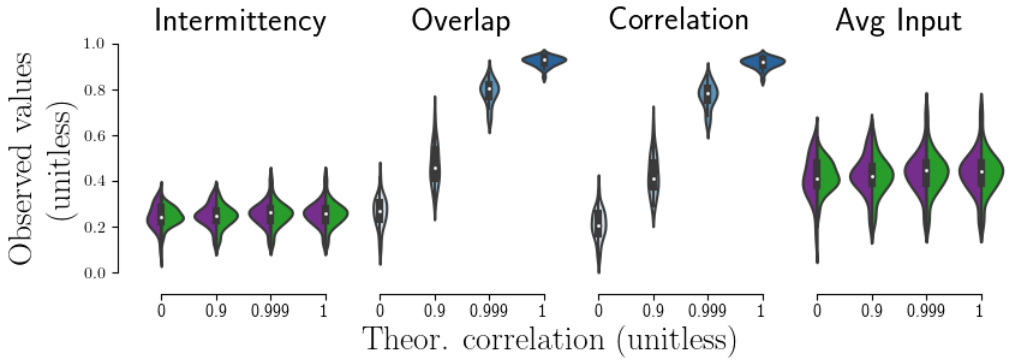

Figure 8–Figure supplement 1. Observed properties of the simulated plumes as a function of the intended correlation between plumes averaged over 200 s. Intermittency and average input plots show the values for the two plumes (green and purple).

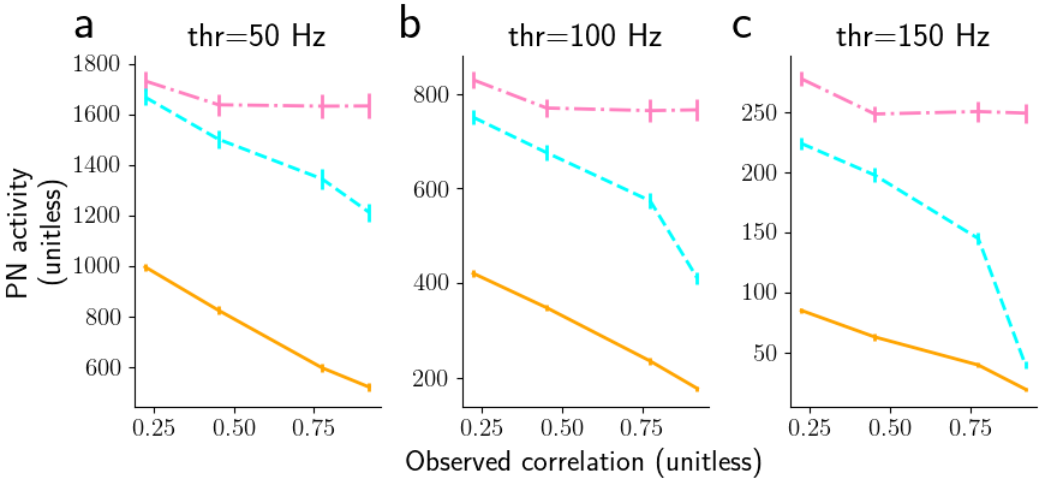

Figure 8–Figure supplement 2. Panels a-c) show the total PN activity above 50, 100, 150 Hz, respectively, for 3 ms maximum whiff durations.

bioRxiv preprint doi: https://doi.org/10.1101/2020.07.23.217216; this version posted July 24, 2020. The copyright holder for this preprint (which was not certified by peer review) is the author/funder, who has granted bioRxiv a license to display the preprint in perpetuity. It is made available under a CC-BY 4.0 International license.

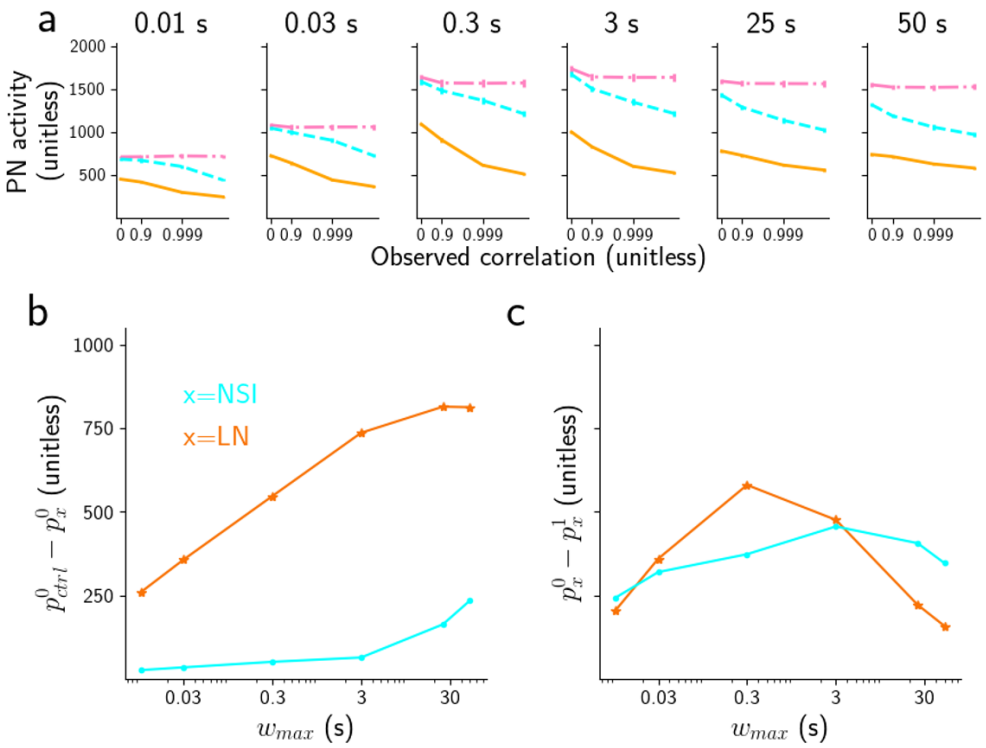

Figure 9–Figure supplement 1. a) peak PN threshold $50\,\mathrm{Hz}$ for different subsets of whiff durations (from 0.01 to $50\,\mathrm{s}$) for the three models: control model (dot dashed pink), LN model (orange continuous), and NSI model (dashed cyan). Note that the horizontal axis has a log-scale.

bioRxiv preprint doi: https://doi.org/10.1101/2020.07.23.217216; this version posted July 24, 2020. The copyright holder for this preprint (which was not certified by peer review) is the author/funder, who has granted bioRxiv a license to display the preprint in perpetuity. It is made available under a CC-BY 4.0 International License.

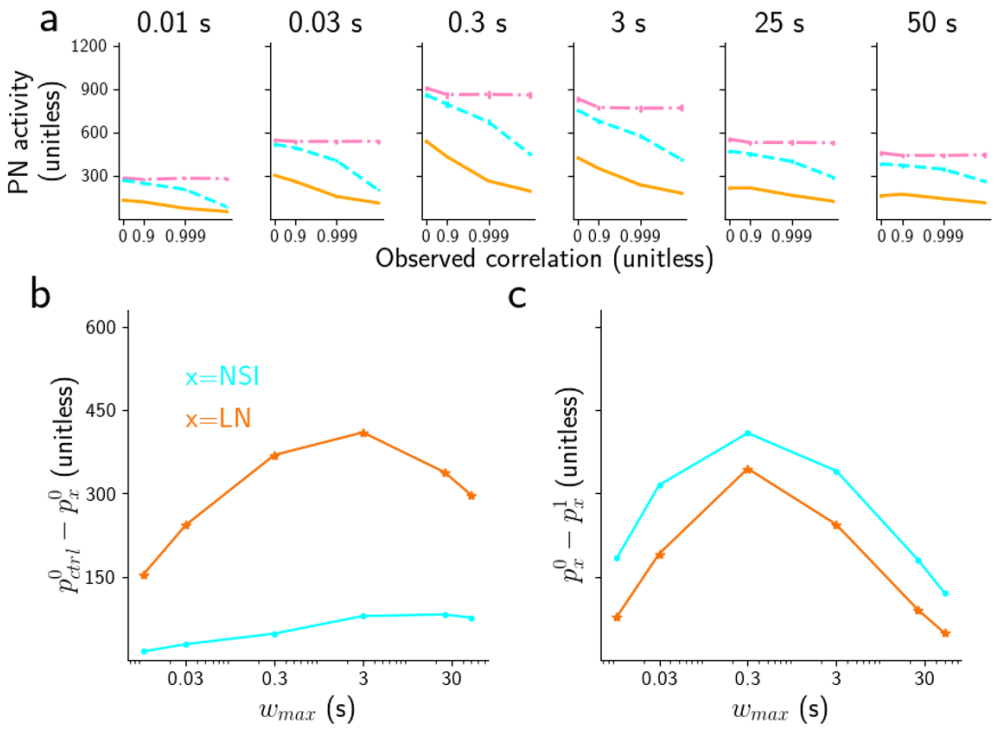

Figure 9–Figure supplement 2. a) peak PN threshold $100\,\mathrm{Hz}$ for different subsets of whiff durations (from 0.01 to $50\,\mathrm{s}$) for the three models: control model (dot dashed pink), LN model (orange continuous), and NSI model (dashed cyan). Note that the horizontal axis has a log-scale.